Journal of Controlled Release 359 (2023) 384–399

Contents lists available at ScienceDirect

Journal of Controlled Release

journal homepage: www.elsevier.com/locate/jconrel

Effective nose-to-brain drug delivery using a combination system targeting the olfactory region in monkeys

Keita Sasaki [a], Shota Fukakusa [a,b], Yusuke Torikai [a], Chie Suzuki [b], Ikumi Sonohata [c], Takuto Kawahata [a], Yasuhiro Magata [b], Keiichi Kawai [d,e], Shunji Haruta [a,*]

[a] R&D Department, TR Company, Shin Nippon Biomedical Laboratories, Ltd., 2438 Miyanoura, Kagoshima 891-1394, Japan
[b] Department of Molecular Imaging, Institute for Medical Photonics Research, Preeminent Medical Photonics Education & Research Center, Hamamatsu University School of Medicine, 1-20-1 Handayama, Higashi-ku, Hamamatsu 431-3192, Japan
[c] Department of Pathology, Drug and Safety Research Laboratories, Shin Nippon Biomedical Laboratories, Ltd., 2438 Miyanoura, Kagoshima 891-1394, Japan
[d] Faculty of Health Sciences, Institute of Medical, Pharmaceutical and Health Sciences, Kanazawa University, 5-11-80 Kodatsuno, Kanazawa 920-1192, Japan
[e] Biomedical Imaging Research Center, University of Fukui, 23-3 Matsuokashimoaizuki, Eiheiji, Yoshida-gun, Fukui 910-1193, Japan

ARTICLE INFO

Keywords:
Nose-to-brain drug delivery
Combination delivery system
Olfactory region
3D-printed nasal cast
Cynomolgus monkeys
[^{18}F]Fallypride

ABSTRACT

The nose-to-brain (N2B) pathway has garnered attention because it transports drugs directly into the brain. Although recent studies have suggested the necessity of selective drug administration to the olfactory region for effective N2B drug delivery, the importance of delivering the formulation to the olfactory region and the detailed pathway involved in drug uptake in primates brain remain unclear. Here, we developed a combination system for N2B drug delivery comprising a proprietary mucoadhesive powder formulation and a dedicated nasal device (N2B-system) and evaluated it for nasal drug delivery to the brain in cynomolgus monkeys. This N2B-system demonstrated a much greater formulation distribution ratio in the olfactory region in an in vitro experiment using a 3D-printed nasal cast and in vivo experiment using cynomolgus monkeys, as compared to that in other nasal drug delivery systems that comprise of a proprietary nasal powder device developed for nasal absorption and vaccination and a commercially available liquid spray. Additionally, Texas Red-labeled dextran (TR-DEX, 3 kDa) was administered using the N2B-system to estimate the drug transition pathway from the nasal cavity to the brain. TR-DEX preferentially localized to the olfactory epithelium and reached the olfactory bulb through the cribriform foramina. Moreover, domperidone, a model drug with poor blood-brain barrier permeability, was administered to assess the brain uptake of medicine after olfactory region-selective administration by using the N2B-system. Domperidone accumulation in the brain was evaluated using positron emission tomography with intravenously administered [^{18}F]fallypride based on competitive inhibition of the dopamine D2 receptor (D2R). Compared to other systems, the N2B-system significantly increased D2R occupancy and domperidone uptake in the D2R-expressing brain regions. The current study reveals that the olfactory region of the nasal cavity is a suitable target for efficient nasal drug delivery to the brain in cynomolgus monkeys. Thus, the N2B-system, which targets the olfactory region, provides an efficient approach for developing effective technology for nasal drug delivery to the brain in humans.

1. Introduction

The blood-brain barrier (BBB) plays a critical role in protecting the central nervous system (CNS) from potentially harmful exogenous substances [1]. However, it is a major obstacle to delivering CNS therapeutics to the brain following systemic administration [2]. In recent decades, extensive studies have been conducted on intranasal (IN) administration as a technique to efficiently deliver drugs with poor BBB permeability, such as biologics [3–5], nucleic acid therapeutics [6], and P-glycoprotein (P-gp) substrates [7,8] into the brain. In particular, the nose-to-brain (N2B) pathway is of scientific interest because it bypasses the BBB to transport medicines directly and noninvasively into the brain [9,10]. The N2B drug delivery pathway has two proposed primary routes of drug transport through the nasal epithelium toward the brain, i.e., the olfactory and trigeminal routes [11]. The dominant N2B drug delivery pathway is the olfactory route located on the roof of the nasal

* Corresponding author.
E-mail address: haruta.shunji@snbl.com (S. Haruta).

https://doi.org/10.1016/j.jconrel.2023.06.005
Received 11 April 2023; Received in revised form 1 June 2023; Accepted 3 June 2023
Available online 16 June 2023

cavity in the olfactory region [12]. Recent studies have developed techniques to administer drugs selectively and reliably through the olfactory region in rodents [13,14]. These methodological advancements have demonstrated the significance of selective olfactory dosing for highly effective nasal drug delivery to the brain. However, the olfactory region of the nasal cavity in rodents has a greater occupancy rate than that in humans. This could lead to an overestimation of the drug uptake amount into the brain through the N2B pathway in humans [15]. Owing to their genetic homology and physical resemblance to humans, non-human primates, such as the cynomolgus monkey (*Macaca fascicularis*), are commonly employed in preclinical investigations. Furthermore, the cynomolgus monkey is more similar to humans in nasal anatomy and occupancy rate of the olfactory region in the nasal cavity than to other experimental animals [11,16,17].

Our previous study demonstrated the development of a combination drug delivery system for nasal drug absorption and vaccination (Abs-system) comprising an inactive nasal powder carrier with mucoadhesive properties and a nasal device (Fit-lizer™ Type A for Non-Human Primates, A-device) in conscious cynomolgus monkeys. The Abs-system efficiently and noninvasively delivered dry powder formulations to the respiratory region of the nasal cavity. Moreover, the Abs-system with oxytocin and ovalbumin-antigen resulted in faster systemic absorption and greater mucosal immunogenicity than in a commercially available liquid spray system [5,18]. However, the Abs-system showed a limited formulation distribution to the olfactory region due to complicated factors, including system requirements and nasal cavity structure. Therefore, the Abs-system might be unsuitable for nasal drug delivery to the brain via the olfactory route, and more trials with the combination system comprising nasal formulations and nasal devices are necessary to determine the optimal conditions for efficient N2B drug delivery.

In the present study, a new combination system for N2B drug delivery (N2B-system) comprising an existing mucoadhesive nasal carrier and a newly designed nasal device (N2B-device) was developed for its suitability for drug delivery to the olfactory region and efficiency of nasal drug uptake into the brain of cynomolgus monkeys. First, to investigate whether the newly developed N2B-system achieved efficient delivery to the olfactory region, the N2B-system was evaluated for formulation delivery characteristics. Second, the distribution pattern of the formulation delivered by the N2B-system was confirmed using a three-dimensional (3D)-printed nasal cast and in live monkeys. Finally, to evaluate the effectiveness of N2B drug delivery through olfactory region-selective administration, Texas Red-labeled dextran (TR-DEX, 3 kDa) and domperidone, which have poor BBB-permeability [19,20], were administered to conscious monkeys using the N2B-system.

2. Materials and methods

2.1. Animals

All animal experiments, except for the positron emission tomography (PET) imaging study, were approved by the Institutional Animal Care and Use Committee of Shin Nippon Biomedical Laboratories, Ltd. (approval no. IACUC996–204, −229, and − 233), a facility fully certified by The Association for Assessment and Accreditation of Laboratory Animal Care International (AAALAC). The PET imaging study was conducted in compliance with institutional and national animal care norms and approved by the Animal Care and Use Committee of the Hamamatsu University School of Medicine (Approval No. 2019040). Twenty male cynomolgus monkeys [purpose-bred, B-virus antibody negative; Shin Nippon Biomedical Laboratories (SNBL), Ltd., Kagoshima, Japan] that were 4–6 years of age and weighed 4.42–7.05 kg were used. All monkeys were fed approximately 108 g of commercial solid food (HF Primate J 12G 5K9J, Purina Mills, LLC., MO, USA or Certified Primate Diet 5048, LabDiet, MO, USA) once a day with tap water ad libitum from an automatic water supply. They were kept in an environmentally controlled room under the following conditions: temperature, 26 ± 3 °C; humidity, 50% ± 20%; ventilation, 15 times/h; and a 12 h light/dark cycle (lighting from 07:00 a.m.).

2.2. Formulations

The yellow dye tartrazine was purchased from FUJIFILM Wako Pure Chemical Corp. (Osaka, Japan). Manganese chloride tetrahydrate ($MnCl_2{\cdot}4H_2O$) was purchased from Sigma-Aldrich (MO, USA). Texas Red-labeled 3 kDa dextran and lysine fixable (TR-DEX) were purchased from Thermo Fisher Scientific (Waltham, MA, USA). Domperidone maleate was purchased from Toronto Research Chemicals Inc. (Toronto, Canada). Powder formulations were prepared by mortar mixing each of the above substances with a proprietary carrier that included a specific type of microcrystalline cellulose as the main component (Ceolus® PH grade, Asahi Kasei Corp., Tokyo, Japan). The powder formulations used in the in vitro nasal distribution trial with a 3D-printed nasal model contained the yellow dye and had the following composition (yellow dye/carrier): 1.0 mg/24.0 mg, 1.5 mg/36.0 mg, 2.0 mg/48.0 mg and 3.0 mg/72.0 mg. The powder formulation with manganese used in the in vivo nasal distribution trial using living monkeys was composed of 1.0 mg of $MnCl_2{\cdot}4H_2O$/24.0 mg of the carrier. For the immunohistological assessment of the nasal cavity, the powder formulation with TR-DEX had the following composition: 10.0 mg of TR-DEX/15.0 mg of the carrier. For PET imaging in living monkeys, the powder formulation with domperidone (domperidone maleate [an equivalent dose of domperidone-free base]/the carrier) used had the following composition: 2.1 mg (1.6 mg)/22.9 mg, 6.6 mg (5.0 mg)/18.4 mg, and 19.8 mg (15.0 mg)/17.7 mg. For delivery characteristics, nasal deposition, and PET imaging studies, the powder formulation without any substances (placebo powder formulation) had the following composition: 25 mg of the carrier. Liquid formulations were prepared by dissolving each of the mentioned substances in 1% (*w/v*) carboxymethyl cellulose (CMC) saline solvent, which was composed of sodium carboxymethyl cellulose (Cat No. 039–01335, Lot No. LEE6873, FUJIFILM Wako Pure Chemical Corp., Osaka, Japan) and physiological saline (Otsuka Pharmaceutical Factory, Tokushima, Japan). The liquid formulation with the yellow dye contained 1.0 mg of the yellow dye per 100 μL of the solvent. The liquid formulation with manganese contained 1.0 mg of $MnCl_2{\cdot}4H_2O$ per 100 μL of the solvent. The liquid formulation with TR-DEX contained 10.0 mg of TR-DEX per 100 μL of solvent. The liquid formulation with domperidone contained 6.6 mg (5.0 mg) of domperidone maleate (an equivalent dose of domperidone-free base) per 100 μL of the solvent. The liquid formulation with 100 μL of the solvent and without any of the above substances (placebo liquid formulation) was used for studying the delivery characteristics.

2.3. Nasal delivery devices

To deliver the prepared powder formulations, a nasal device (A-device), which was originally developed for IN drug absorption and vaccination (Fit-lizer™ Type A, SNBL) as described previously [5,18], and the N2B-device shown in Fig. 1, which was newly developed for the present N2B study (SNBL), were used. The existing combination drug delivery system comprising the powder formulation and A-device is referred to as the Abs-system. For the A-device, a hydroxypropyl methylcellulose capsule filled with the powder formulation was placed in the capsule holder, and both ends of the capsule were cut off with the built-in cutter. >95% of the powder formulation was delivered from the A-device through the holes of the capsule with air that was supplied by actuating the device pump. The newly developed combination system for N2B drug delivery comprising the powder formulation and the N2B-device is called the N2B-system. For the N2B-device, >95% of the powder formulation contained in the device container was delivered from the device with a specific amount of mechanically generated compressed air at the press of an actuation switch. The N2B-device enables the generation of a higher maximum air pressure and lower air

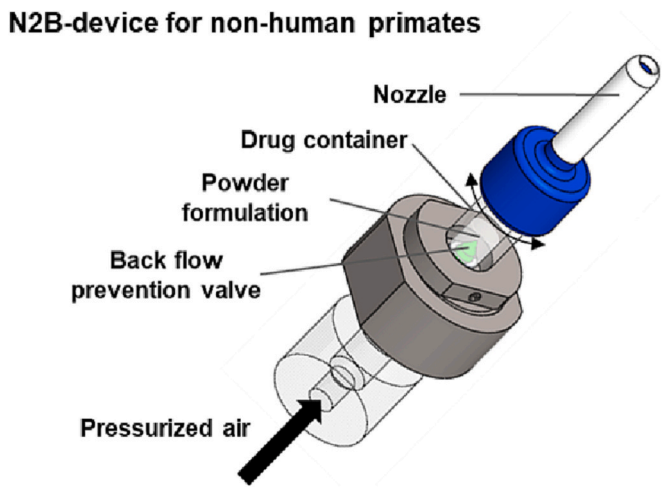

Fig. 1. An illustration of the original N2B-device. Pressurized air was generated by an air compressor supplied with an air controller consisting of a pressure regulator and air volume controller. The controls were set at the appropriate levels for pressurized air-mediated N2B drug delivery (injection pressure = 0.06 MPa; air volume = 9 mL in this study). Pressurized air was sent into the N2B-device to deliver the proprietary powder formulation stored in the rechargeable drug container.

volume (0.06 MPa and 9.0 mL) than those of the A-device (0.03 MPa and 13 mL, respectively). Additionally, to deliver the liquid formulations, the commercially available nasal sprayer MAD Nasal™ Intranasal Mucosal Atomization Device (hereafter referred to as "Liquid spray"; Teleflex Inc., NC, USA) was used. For convenience, the commercially available nasal liquid delivery system comprising the liquid formulation and liquid spray is referred to as the Liquid-system in this study. The liquid formulations in the syringe of the Liquid spray device were delivered by pressing the plunger of the device.

2.4. Delivery characteristics

Plume geometry and spray pattern were the major parameters used to characterize the shapes of the placebo formulation (25 mg of powder carrier or 100 μL of 1% CMC in saline) delivered by each systems. These parameters were measured using the SprayVIEW® measurement system (Proveris Scientific Corporation, MA, USA). For plume geometry measurement, the plume angle and width were determined using a laser sheet placed 3 cm above the nozzle tip of the device oriented vertically with the direction of the formulation delivered from the device. For spray pattern measurement, the spray area was determined using a laser sheet placed 3 cm above the nozzle tip of the device oriented horizontally in the direction of the formulation delivered from the device. Additionally, the duration and peak time associated with the plume intensity of the formulation delivered from the device was measured using passes across the laser sheet. All images of plume geometry and spray pattern measurements were captured at 500 fps. Five replicate measurements were performed for each placebo formulation under ambient conditions. The median secondary particle size (Dv_{50}) of the formulation (placebo powder and liquid formulations) delivered by each system was measured 3 cm above the nozzle tip of the device using the Spraytech® system using a laser diffraction particle size analyzer (Malvern Panalytical, Ltd., Malvern, England).

2.5. 3D-printed nasal cast

A 3D-printed nasal cast, a highly accurate model design based on computed tomography/magnetic resonance imaging (MRI) of a cynomolgus monkey, was prepared previously [18]. The 3D-printed nasal cast was divided into four regions: nasal vestibule, respiratory region, olfactory region, and nasopharynx; and the surface areas and occupancy ratios were as follows: 7.48 mm^2 and 19.45%, 17.44 mm^2 and 45.33%, 2.87 mm^2 and 7.45%, and 10.68 mm^2 and 27.77%, respectively.

2.6. Measurement of tartrazine (yellow dye) and method validation

Prior to the measurement of yellow dye deposition in the 3D-printed nasal cast, the analytical method validation was performed to ensure the suitability of the high-performance liquid chromatography (HPLC) for the measurement of tartrazine distributed on the 3D-printed nasal cast. The method's specificity, linearity, repeatability, and stability of the analytical solution were validated. The Shimadzu HPLC system (Shimadzu Prominence-i LC-2030C 3D Plus; Kyoto, Japan) was employed for analyzing the standard solutions of the analyte. The mobile phase consisted of a 10 mM sodium dihydrogen phosphate buffer and acetonitrile (90:10, *v*/v), which flowed through a column (C18; Inertsil ODS-3; 150 mm × 4.6 mm, i.d., 5 μm, GL Sciences Inc., Tokyo, Japan) at a rate of 1.0 mL/min and at a temperature of 40 °C. The concentration of the yellow dye was determined at 427 nm using a UV detector. For the specificity, no interfering peaks were observed at the retention time of the tartrazine peak. The linearity of the standard curve was confirmed within the ranges of 1 to 30 μg/mL and 30 to 100 μg/mL of tartrazine. The relative deviation for each standard curve ranged from 0.0% to 0.3% and 0.1% to 0.4%, respectively, and the correlation coefficient (r) for each standard curve was above 0.999. For repeatability, the relative standard deviation of six injections was taken twice and found to be 0.05% and 0.10%. For the solution stability, the standard solutions were found to be stable in the autosampler for 24 h. Additionally, the recovery ratio was evaluated thrice to ensure the retrieval method of the tartrazine formulation from the 3D-printed nasal cast for the assay of tartrazine in IN formulation. The powder formulation of 2 mg containing 0.1 mg tartrazine was directly applied to each section of the 3D-printed nasal cast (nasal vestibule, olfactory region, respiratory region, and nasopharynx) and then retrieved using distilled water. The mean recovery ratio and relative standard deviation for each section were >90% and <8%, respectively. Furthermore, no interfering peaks at the retention time of tartrazine were observed when the same procedure was performed using the placebo formulation.

2.7. In vitro nasal formulation distribution and deposition in the 3D-printed nasal cast

To evaluate the nasal distribution and deposition of the formulation, we delivered the formulation with yellow dye by each system into the 3D-printed nasal cast through one nostril, which had a semi-wet-treated inner wall that was equivalent to the nasal mucosa due to artificial saliva coating (Saliveht Aerosol, Teijin. Pharma Ltd., Tokyo, Japan). The yellow dye (1 mg) was delivered at a total volume consisting of 25 mg of the powder formulation and 100 μL of the liquid formulation using the Abs-system and Liquid-system, respectively. Doses of 1, 1.5, 2, and 3 mg of yellow dye were delivered at total volumes of 25.0, 37.5, 50.0, and 75.0 mg of the powder formulation using the N2B-system, respectively. After delivery into the 3D-printed nasal cast, the formulation distributed in each region was recovered using 10 mL of distilled water. A sample solution containing the yellow dye was prepared by mixing and filtering the recovered solution or suspension. The sample solution was diluted in a mixture of phosphate buffer (10 mM sodium dihydrogen phosphate buffer, pH 6.9) and acetonitrile (90:10 *v*/v). The diluted sample measured for tartrazine (yellow dye) was done using the described HPLC analytical method. The lower limit of quantification (LLOQ) was defined as 1 μg/mL.

2.8. In vivo nasal formulation distribution and Mn^{2+} uptake in olfactory bulb using Manganese-Enhanced MRI (MEMRI)

MRI was performed using a 3.0 T MAGNETOM Trio (Siemens,

Erlangen, Germany) equipped with a 32-channel receiver coil designed for human head imaging. MEMRI images were acquired in the sagittal plane using a 3D magnetization-prepared rapid gradient-echo sequence (MPRAGE) with TR, 2000 ms; TE, 3.34 ms; slice thickness, 0.5 mm; and flip angle, 12° at each time point (before and approximately 20 min, 3 h, 6 h, and 24 h after dosing each formulation). Conscious monkeys received the formulation with manganese at a dose of 1 mg $MnCl_2{\cdot}4H_2O$ using each system into the right nostril ($n = 3$/each group). For imaging, the monkeys were anesthetized with ketamine hydrochloride (50 mg/mL, 0.3 mL/kg, Ketalar for intramuscular injection, Daiichi-Sankyo, Japan), and medetomidine hydrochloride (1 mg/mL, 0.08 mL/kg, Domitor, Orion Corporation, Finland) immediately after IN administration. The MRI images were analyzed to evaluate the nasal distribution and accumulation of Mn^{2+} in the olfactory bulb using OSIRIX MD 12.5.2 (Pixmeo, Bernex, Switzerland). The percentage signal intensity in the ipsilateral olfactory bulb was calculated using the following equation: % signal intensity = $[(\text{Ipsilateral}_{\text{time}}/\text{Contralateral}_{\text{time}})/(\text{Ipsilateral}_{\text{pre}}/\text{Contralateral}_{\text{pre}})] \times 100$.

2.9. Nasal formulation deposition and TR-DEX uptake in the nasal cavity

Histological examinations were performed to evaluate the detailed distribution and deposition of the placebo formulation (25 mg powder carrier) in monkeys. Conscious monkeys received the placebo formulation using the Abs-system or N2B-system into the right nostril ($n = 2$/each group) 30 min and 6 h before collection of the nasal cavity. Detailed fluorescence imaging was performed to evaluate the distribution and cellular uptake of TR-DEX in the nasal cavity. Conscious monkeys received a dose of 10 mg TR-DEX using the A-system and N2B-system in the right nostril (n = 2/each group) 30 min before collection of the nasal cavity.

2.10. Nasal cavity collection and tissue preparation

Under deep pentobarbital anesthesia (64.8 mg/mL, 0.4 mL/kg, IV; Tokyo Chemical Industry, Tokyo, Japan), the monkeys were injected with heparinized saline into the cephalic vein and perfused transcardially with approximately 1 L ice-cold saline followed with approximately 1 L of a 4% paraformaldehyde (PFA) solution (Sigma-Aldrich Co. LLC). The nasal cavities were isolated, post-fixed for 24 h in 4% PFA, and decalcified in 10% formic acid solution (Kanto Chemical, Tokyo, Japan) for approximately one week. After decalcification, the nasal cavities were cut into two blocks (the olfactory region with the olfactory bulb, and the respiratory region). The tissue blocks were quickly frozen in Tissue-Tek® O.C.T. Compound (Sakura Finetek Japan, Tokyo, Japan) using liquid nitrogen and stored at −80 °C until used later. The nasal cavity tissue was cut on a cryostat (Leica Biosystems, Nussloch, Germany) to a thickness of 30 μm, and the sections were directly mounted on an adhesive film (Cryofilm type 2C; Section-lab, Hiroshima, Japan) with a glass slide. The slides were stored at −80 °C until used later.

2.11. Histology and immunohistochemistry of the olfactory and respiratory regions

The nasal tissue slides were stained with Alcian blue 8XG solution and nuclear fast red solution (Merck KGaA, Darmstadt, Germany) according to the manufacturer's instructions. Briefly, the slides were washed twice with distilled water (5 min each), immersed in 3% acetic acid solution (2 min) and stained with Alcian blue solution (15 min). After rinsing in 3% acetic acid solution (5 min × 2 times) and running tap water (2 min), the tissue sections were counterstained with a nuclear fast red solution (5 min), dehydrated, and mounted using EUKITT® neo mounting medium (ORSAtec, Bobingen, Germany). Additionally, the unstained specimens directly mounted with cover glass were observed to prevent the removal of the powder formulation adhered to the olfactory mucosa. Immunohistochemical staining was performed on the nasal tissue sections washed with TBST (0.1% Triton X-100 in TBS). The slides were incubated for 3 h with a blocking buffer containing 3% bovine serum albumin in TBST and subsequently allowed to react with mouse anti-olfactory marker protein (OMP) antibody (1:500, B-6, #sc-365,818, Santa Cruz Biotechnology, TX, USA), mouse anti-fibronectin antibody (1:500, #ab6328, Abcam, Cambridge, UK), or rabbit anti-PGP9.5 antibody (1:500, EPR4118, #ab108986, Abcam) overnight at 4 °C. After washing, the slides were incubated with the secondary antibodies Alexa 488-conjugated anti-mouse IgG_{2a}, anti-mouse IgG, or anti-rabbit IgG (1:1000; Invitrogen, CA, USA) for 2 h at 23 °C. After further washing and nuclear staining with Hoechst 33342 (1:5000, Dojindo, Kumamoto, Japan), the slides were mounted using VECTASHIELD Mounting Medium (Vector Laboratories, CA, USA) and analyzed using a fluorescence microscope (BZ-X800, Keyence, Osaka, Japan).

2.12. Acquisition of the brain MRI image for nasal tissue collection and PET imaging

The monkeys were anesthetized with 0.3 mL/kg ketamine hydrochloride (50 mg/mL) and 0.08 mL/kg medetomidine hydrochloride (1 mg/mL). MRI was performed on a 3.0 T MAGNETOM Trio with a 3D MPRAGE sequence, as described earlier, and brain MRI images were acquired to provide anatomical information for nasal tissue collection. Brain MRI images were also acquired for use as the brain template for PET imaging using a 3.0 T MAGNETOM Trio with a 3D MPRAGE sequence or a 3.0 T Signa HDxt (GE Healthcare, Milwaukee, WI, USA) with a 3D T1-weighted fast spoiled gradient-recalled sequence (TR, 12.64 ms; TE, 5.58 ms; slice thickness 0.5 mm; and 12° flip angle).

2.13. [^{18}F]Fallypride PET imaging

Fluorine-18 was produced by $^{18}O(p, n)^{18}F$ nuclear reaction using a 12 MeV cyclotron (CYPRIS® HM-12, Sumitomo Heavy Industry, Tokyo, Japan). [^{18}F]Fallypride was radiosynthesized using a multipurpose synthesizer MPS-100 (Sumitomo Heavy Industries), as previously described [21] with slight modifications. Briefly, the labeling precursor (Tosyl-Fallypride; ABX Advanced Biochemical Compounds, Radeberg, Germany) was made to react with tetrabutylammonium [^{18}F]fluoride in acetonitrile at 100 °C for 10 min. [^{18}F]Fallypride was purified using HPLC with a COSMOSIL 5-C18-AR-II packed column (10 × 250 mm, Nacalai Tesque, Kyoto, Japan) using 0.6% triethylamine in 70% acetonitrile as the mobile phase, dried, and reconstituted with 5 mL of saline. At the end of synthesis, the radiochemical purity and molar activity of [^{18}F]fallypride were determined to be >97% and 475.7 GBq/μmol using HPLC with a COSMOSIL 5-C18-AR-II packed column (4.6 × 150 mm, Nacalai Tesque, Japan) using a mixture of acetonitrile and 0.1 M ammonium formate (60/40, *v*/v) as the mobile phase. The monkeys were fasted for at least 12 h before PET imaging. Conscious monkeys received the formulations at a dose of 5 mg domperidone using the Liquid-system and Abs-system and the powder formulations at doses of 0 (placebo powder formulation, as a control group), 1.6, 5, and 15 mg domperidone using the N2B-system ($n = 3$/each group) 30 min before PET imaging. The monkeys were initially anesthetized with 4% isoflurane in an air–O_2 mixture and placed in the supine position with a head fixation holder. The body temperature was maintained using a heating pad at 37 °C (GAYMAR T/Pump System Localized Warming Therapy, Stryker, MI, USA). Vital signs (heart rate, electrocardiogram, blood pressure, body temperature, respiratory rate, and percutaneous oxygen saturation) were monitored using a bedside monitor (Life scope BSM-3592, Nihon Kohden, Tokyo, Japan) during anesthesia for the PET scan. Venous blood was collected from the femoral vein to measure the plasma concentration of domperidone before injecting [^{18}F]fallypride. [^{18}F]Fallypride (~171.3 MBq) dissolved in up to 0.5 mL of saline was administered as an intravenous bolus via the indwelling saphenous vein cannula, and the subsequent heparinized saline was flashed into the monkeys. Immediately at the start of [^{18}F]fallypride injection, dynamic

PET scans were performed for 3 h using a HITS-655 K PET scanner (Hamamatsu Photonics KK, Hamamatsu, Japan) under anesthesia with 1.5–2.0% isoflurane in an air–O_2 mixture until the end of the PET scan. Four iterations of PET images with attenuation and scatter corrections were reconstructed using the list-mode dynamic row action maximum likelihood algorithm with a time frame of 10 × 1 min/frame and subsequently at 17 × 10 min/frame [22].

2.14. PET image analyses

The volume of interest (VOI) of the target regions (F. CTX, frontal cortex; Cd, caudate; Pt, putamen; Amy, amygdala; GP, globus pallidus; SN/VTA, substantia nigra/ventral tegmental area; Thal, thalamus; PAG, periaqueductal gray) and the reference region (cerebellum) were preset on the MRI images and defined for each region for each hemisphere using the Amide (exe 1.0.4) free software program (https://amide.sourceforge.net/). The mean standardized uptake value (SUV_{means}) was calculated in each region as a quantitative assessment of [^{18}F]fallypride accumulation using the following equation: SUV = [mean radioactive concentration in VOI (MBq/mL)/injected dose (MBq)] × body weight (g). The specific uptake of [^{18}F]fallypride was calculated by subtracting the SUV of the cerebellum as a reference region from that of the target regions. The binding potential (BP_{ND}) in each target region was determined using Logan graphical analysis using the cerebellum as a reference region (t^* = 80 min) [23]. The percentage of D2R occupancy (*%RO*) by domperidone was determined using the BP_{ND} obtained from the control group ($BP_{ND(Cont)}$) and domperidone treatment group ($BP_{ND\ (Dom)}$) as follows: $\%RO = [1 - BP_{ND\ (Dom)}/BP_{ND\ (Cont)}] \times 100$. Increasing *%RO* was used as an indicator of the degree of domperidone occupancy of its D2R in the brain. Mean *%RO* maps were generated to visually compare the differences between each experimental group using the PMOD software program v4.3 (PMOD Technologies LLC, Zurich, Switzerland). First, individual [^{18}F]fallypride PET/MRI images were spatially normalized to the adjunctive template brain atlas using the PMOD Neuro tool (PNEURO), and individual BP_{ND} maps were obtained through voxel-by-voxel calculations using the Logan method described above. Next, the individual voxel-by-voxel *%RO* was calculated to generate the *%RO* maps (n = 3).

2.15. Measurement of plasma domperidone concentrations

Measurement of plasma domperidone concentrations was outsourced to Kamakura Techno-Science, Inc. (Kanagawa, Japan). The assay was validated using liquid chromatography-tandem mass spectrometry (LC-MS/MS). Liquid chromatography was performed using a Shimadzu HPLC system (Nexera X2 LC-30 CE). A C18 analytical column (CAPCELL PAK C18 MGII, 5 μm, 2.0 mm I.D. × 50 mm; OSAKA SODA Co., Ltd., Osaka, Japan) was used at 50 °C. The mobile phase consisted of acetonitrile and 10 mol/L ammonium formate solution set at a flow rate of 0.4 mL/min. Mass spectrometry (MS) was performed using a QTRAP6500 triple-quadruple mass spectrometer (AB Sciex Pte. Ltd., MA, USA) with an electrospray ionization (ESI) interface. The ESI source was set in the positive ionization mode. The MS operating conditions were optimized as follows: scan type, multiple reaction monitoring mode; ion spray voltage, 2500 V; and ion transfer capillary temperature, 700 °C. The LLOQ was defined as 1 ng/mL.

2.16. Statistical analyses

All results are expressed as mean and standard deviation (mean ± SD). Statistical analyses were performed using one-way analysis of variance (ANOVA) or two-way ANOVA with Tukey's multiple comparison *post-hoc* test using the GraphPad Prism 9 statistical software (GraphPad Software, Inc., CA, USA). A p value <0.05 was considered indicative of a significant difference (* $p < 0.05$, ** $p < 0.01$, *** $p < 0.001$, **** $p < 0.0001$).

3. Results

3.1. Delivery characteristic analysis

The characteristics of the placebo formulations delivered by the three systems are listed in Table 1. The plume geometries of the three systems were measured in terms of plume angle and width. Notably, the plume angle and plume width for both the Abs-system and N2B-system were significantly narrower and shorter than those for the Liquid-system ($p < 0.0001$ versus Abs-system and N2B-system). The spray areas for both the Abs-system and N2B-system were significantly smaller than those for the Liquid-system ($p < 0.0001$ versus Abs-system and N2B-system). The spray intensity in the spray pattern analysis was detected from the spray forms of the formulations delivered from each device. It includes the duration of the intensity and peak time to reach the maximum intensity. For the N2B-system, the duration and peak time significantly decreased compared with that of the other systems (duration: $p = 0.0203$ versus Liquid-system, $p = 0.0006$ versus Abs-system; peak time: $p < 0.0001$ versus Liquid-system, $p = 0.0007$ versus Abs-system). The Dv50 of the secondary particle size, median particle size of the delivered formulation, showed a difference between the Liquid-system and both the Abs-system and N2B-system ($p < 0.0001$ versus Abs-system and N2B-system). Moreover, Dv50 slightly differed between the Abs-system and N2B-system ($p = 0.0148$).

3.2. Evaluation of nasal distribution in 3D-printed nasal cast of monkey

The nasal formulation distribution patterns for each system were evaluated using a 3D-printed nasal cast of a cynomolgus monkey [18]. Fig. 2A shows the external appearance of the 3D-printed nasal cast (left, assembled form; right, disassembled form). The 3D-printed nasal cast

Table 1
Delivery characteristics for the systems. Delivery characteristics, including plume geometry, spray pattern, plume intensity, and mean secondary particle size, were evaluated for the three systems.

Measurement	Distance (mm)	Parameter	Device		
			Liquid-system (n = 5)	Abs-system (n = 5)	N2B-system (n = 5)
Plume geometry	30	Plume angle (°)	48.0 ± 9.03	20.5 ± 2.59[a]	24.0 ± 2.18[a]
		Plume width (mm)	27.1 ± 5.62	10.9 ± 1.40[a]	12.8 ± 1.22[a]
Spray pattern		Area (mm^2)	401.9 ± 15.9	95.2 ± 3.52[a]	141 ± 9.10[a,b]
		Ovality (D_{max}/D_{min})	2.34 ± 0.23	1.72 ± 0.08[a]	1.36 ± 0.05[a,c]
Plume intensity		Duration (ms)	97.2 ± 13.97	114 ± 17.11	70.4 ± 6.84[d,e]
		Peak time (ms)	54.8 ± 8.32	38.8 ± 11.37[d]	10.8 ± 5.02[a,e]
Secondary particle size		Dv50 (μm)	246 ± 23.1	1470 ± 68.8[a]	1377 ± 21.9[a,f]

Data are expressed as mean ± standard deviation.
[a] Significantly different from the Liquid-system ($p < 0.0001$, one-way ANOVA with post-hoc Tukey's multiple comparison test).
[b] Significantly different from the Abs-system ($p < 0.0001$, one-way ANOVA with post-hoc Tukey's multiple comparison test).
[c] Significantly different from the Abs-system ($p < 0.01$, one-way ANOVA with post-hoc Tukey's multiple comparison test).
[d] Significantly different from the Liquid-system ($p < 0.05$, one-way ANOVA with post-hoc Tukey's multiple comparison test).
[e] Significantly different from the Abs-system ($p < 0.001$, one-way ANOVA with post-hoc Tukey's multiple comparison test).
[f] Significantly different from the Abs-system ($p < 0.05$, one-way ANOVA with post-hoc Tukey's multiple comparison test).

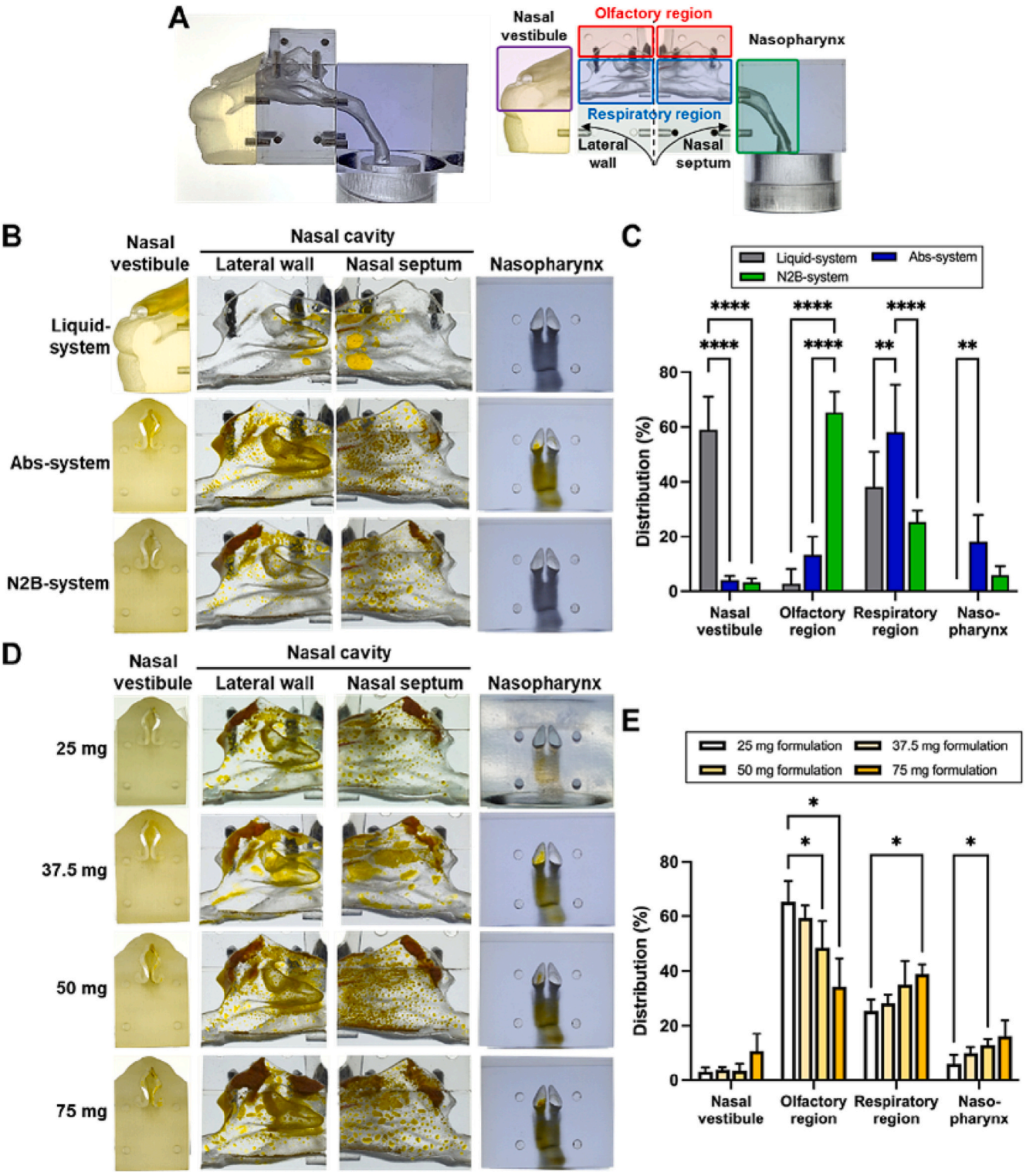

Fig. 2. Distribution of nasal formulations in a 3D-printed nasal cast of a cynomolgus monkey. (A) The external appearance of the 3D-printed nasal cast and disassembled components. The 3D-printed nasal cast is composed of four regions (nasal vestibule, respiratory region, olfactory region, and nasopharynx). (B) Yellow dye deposition using Liquid-system (upper panels), Abs-system (middle panels), and N2B-system (lower panels) in the 3D-printed nasal cast. (C) The percentage of yellow dye distributed using the three systems (** $p < 0.01$, **** $p < 0.0001$). Data are presented as mean ± SD ($n = 5$). (D) Estimation of the appropriate dose volume for selective IN administration to the olfactory region. The yellow dye was delivered using the N2B-system. Typical distribution patterns of powder formulation were administered in four different volumes (25, 37.5, 50, and 75 mg) in the 3D-printed nasal cast. (E) The distribution ratio (%) of yellow dye in the 3D-printed nasal cast is shown (*: $p < 0.05$). Data are given as mean ± SD (n = 5). (For interpretation of the references to colour in this figure legend, the reader is referred to the web version of this article.)

can be divided into four regions: the nasal vestibule, respiratory region, olfactory region, and nasopharynx. This enables the easy retrieval of the formulation with the yellow dye from each region after in vitro formulation delivery test. The representative distribution images of the 25 mg formulation containing 1 mg of the yellow dye delivered using each of the systems in the 3D-printed nasal cast and the percentage of the yellow dye distributed in each region are shown in Fig. 2B and C, respectively. The photographing direction of the nasal vestibule for the Liquid-system was changed to prevent leaks and spills of the liquid formulation. The percentage of yellow dye distributed in the nasal vestibule for the Liquid-system was significantly greater than that for both the Abs-system and N2B-system ($p < 0.0001$ versus Abs-system, $p < 0.0001$ versus N2B-system). The percentage of yellow dye distributed in the olfactory region of the N2B-system was significantly greater than that of the other systems ($p < 0.0001$ versus Liquid-system, $p < 0.0001$ versus Abs-system). In addition, the percentage of yellow dye distributed in the respiratory region for the Abs-system was significantly greater than that for the other systems ($p = 0.0016$ versus Liquid-system, $p < 0.0001$ versus N2B-system). Furthermore, to clarify the appropriate volume of powder formulation for delivery to the olfactory region, we conducted further in vitro formulation distribution studies using the N2B-system with additional volumes of 37.5, 50, and 75 mg of the formulation containing 1.5, 2.0, and 3.0 mg of yellow dye, respectively (Fig. 2D). Although no significant difference was observed in the percentage of yellow dye distributed in the olfactory region at formulation volumes of 25–37.5 mg, the percentage of the yellow dye distributed for volumes ≥50 mg of the formulation was significantly decreased when compared with that for 25 mg of the formulation ($p = 0.0195$ versus 50 mg, $p = 0.0223$ versus 75 mg) (Fig. 2E). These results suggest that the appropriate volume of formulation for delivery with the N2B-system to the olfactory region in living monkeys is up to 37.5 mg/nostril. Therefore, further studies targeting the olfactory region using the N2B-system should consider using this practical dose.

3.3. Evaluation of in vivo formulation distribution in monkey nasal cavity

Previously, we demonstrated that MEMRI imaging is a useful method to easily and non-invasively acquire the in vivo nasal distribution of a formulation containing manganese chloride by detecting the Mn^{2+} signal as a positive contrast agent in living monkeys [18]. MEMRI was performed before (pre) and approximately 20 min, 3 h, 6 h, and 24 h after IN administration (Fig. 3A). The first image acquisition after IN

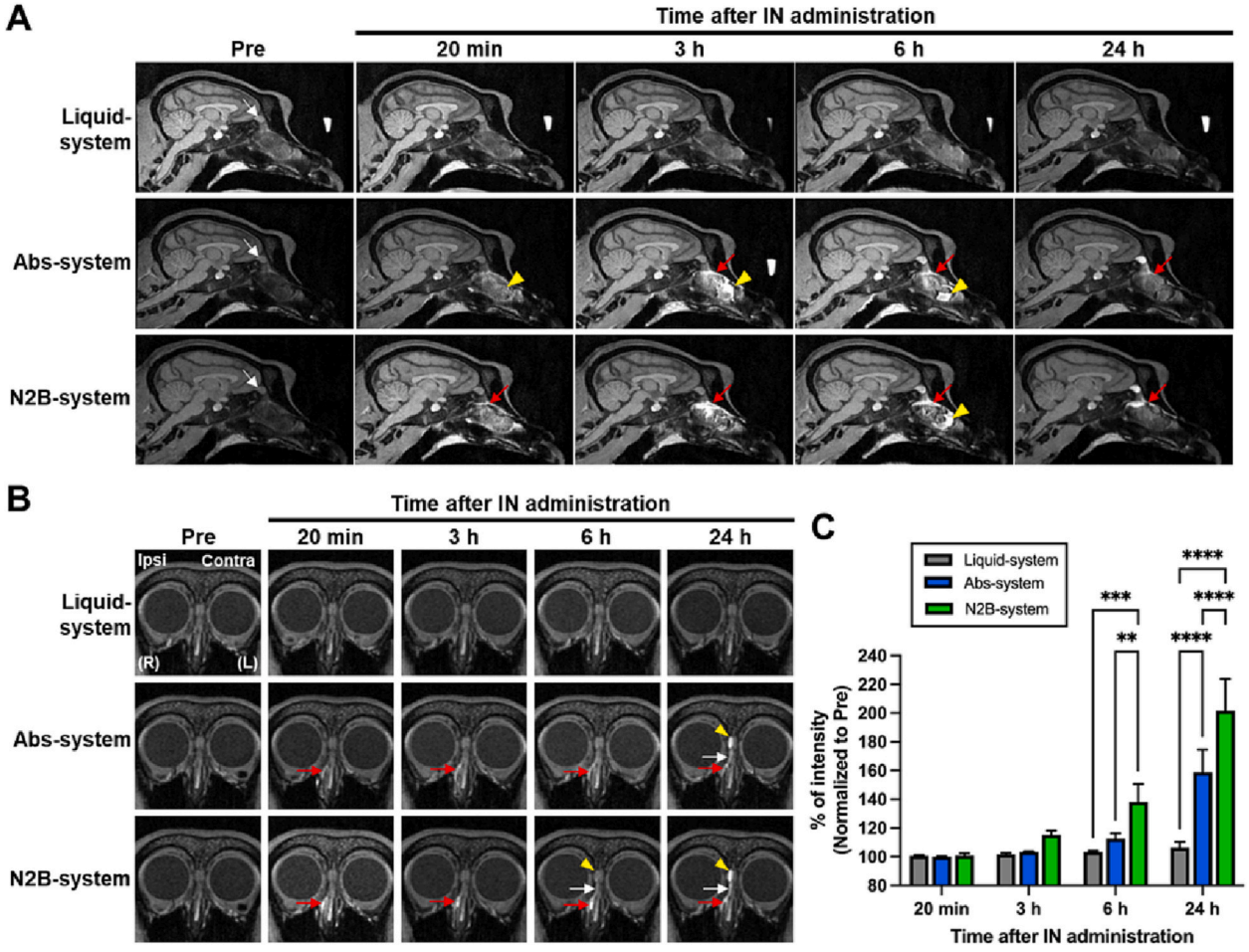

Fig. 3. MEMRI images identify the formulation distribution using Mn^{2+} as an indicator signal. (A) MEMRI images shown as sagittal sections. The MPRAGE sequence images showing the distribution of Mn^{2+} delivered using the Liquid-system (upper panel), the Abs-system (middle panel), and the N2B-system (lower panel) were acquired before (pre) and approximately 20 min, 3 h, 6 h, and 24 h after IN administration. White arrows indicate the location of the olfactory bulb. Yellow arrowheads indicate the Mn^{2+} signals in the respiratory region. Red arrows indicate the distribution of formulation in the olfactory region. (B) Coronal MEMRI images were obtained before (pre) and approximately 20 min, 3 h, 6 h, and 24 h after IN administration. Red arrows indicate the distribution of formulation in the olfactory region. White arrows indicate the Mn^{2+} uptakes into the OSN bundles. Yellow arrowheads indicate the Mn^{2+} accumulation in the ipsilateral olfactory bulb. (C) Time-dependent change of signal intensity (%) in the ipsilateral side of the olfactory bulb was normalized to pre-MEMRI image (** $p < 0.01$, *** $p < 0.001$, **** $p < 0.0001$). Data are given as mean ± SD ($n = 3$). (For interpretation of the references to colour in this figure legend, the reader is referred to the web version of this article.)

administration was set at approximately 20 min because of technical limitations, as previously described [18]. In the Liquid-system, no Mn^{2+} signal could be detected in the nasal cavity at any time point after IN administration. In the Abs-system, Mn^{2+} signals were widely detected, mainly in the respiratory region (yellow arrowhead). In the N2B-system, Mn^{2+} signals were detected mainly in the olfactory region (red arrow). At 24 h after IN administration using both the Abs-system and N2B-system, drastic reduction was observed in Mn^{2+} signal intensity in the respiratory region. In contrast, especially for the N2B-system, Mn^{2+} signal intensity was retained in the olfactory region for 24 h after IN administration.

3.4. Mn^{2+} uptakes in olfactory bulb after IN administration

Recent studies have shown that MEMRI has also been used to evaluate neuronal connectivity and olfactory activity in rodents [24,25]. As is evident from the coronal MEMRI images for the Liquid-system, the ipsilateral Mn^{2+} signal intensity did not change at any time point, unlike the contralateral olfactory bulb (Fig. 3B). For the Abs-system and N2B-system, ipsilateral Mn^{2+} signals were detected in the olfactory region (red arrow) directly below the cribriform plate at all time points after IN administration. In addition, 24 h after IN administration using the Abs-system, Mn^{2+} signals of the ipsilateral olfactory sensory neuron (OSN) bundles (white arrow) and olfactory bulb (yellow arrowhead) showed higher signal intensity than those of the pre-MRI image. Moreover, at 6 h and 24 h after IN administration using the N2B-system, Mn^{2+} signals of the ipsilateral OSN bundles and olfactory bulb showed higher signal intensity than those of the pre-MRI image. Time-dependent changes in the signal intensity in the ipsilateral olfactory bulb are shown in Fig. 3C. Notably, according to the statistical analyses, no significant differences were observed in the signal intensity (%) of the ipsilateral olfactory bulb among the three systems at 20 min and 3 h after IN administration, whereas the N2B-system showed significantly increased signal intensity (%) at 6 and 24 h after IN administration compared with that of the other systems (6 h: $p = 0.0002$ versus Liquid-system, $p = 0.0046$ versus Abs-system; 24 h: $p < 0.0001$ versus Liquid-system and Abs-system).

3.5. Mucoadhesive properties of the powder carrier

To evaluate the in vivo mucoadhesive properties of the powder formulation, the placebo powder formulation was administered intranasally into the nasal cavity using both the Abs-system and N2B-system. Alcian blue/nuclear fast red staining of the nasal mucosa was performed 30 min after IN administration. A small amount of the carrier consisting of the placebo powder formulation (red arrow) was observed for the Abs-system in the ipsilateral olfactory mucosa (Fig. 4A). Unexpectedly, no carriers were observed in the placebo powder formulation on the surface of the respiratory mucosa for the Abs-system, although it was distributed throughout the respiratory region in the 3D-printed nasal cast. These results suggest that the carrier was eliminated from the respiratory mucosa because of highly efficient mucociliary clearance within 30 min of IN administration. However, slight morphological

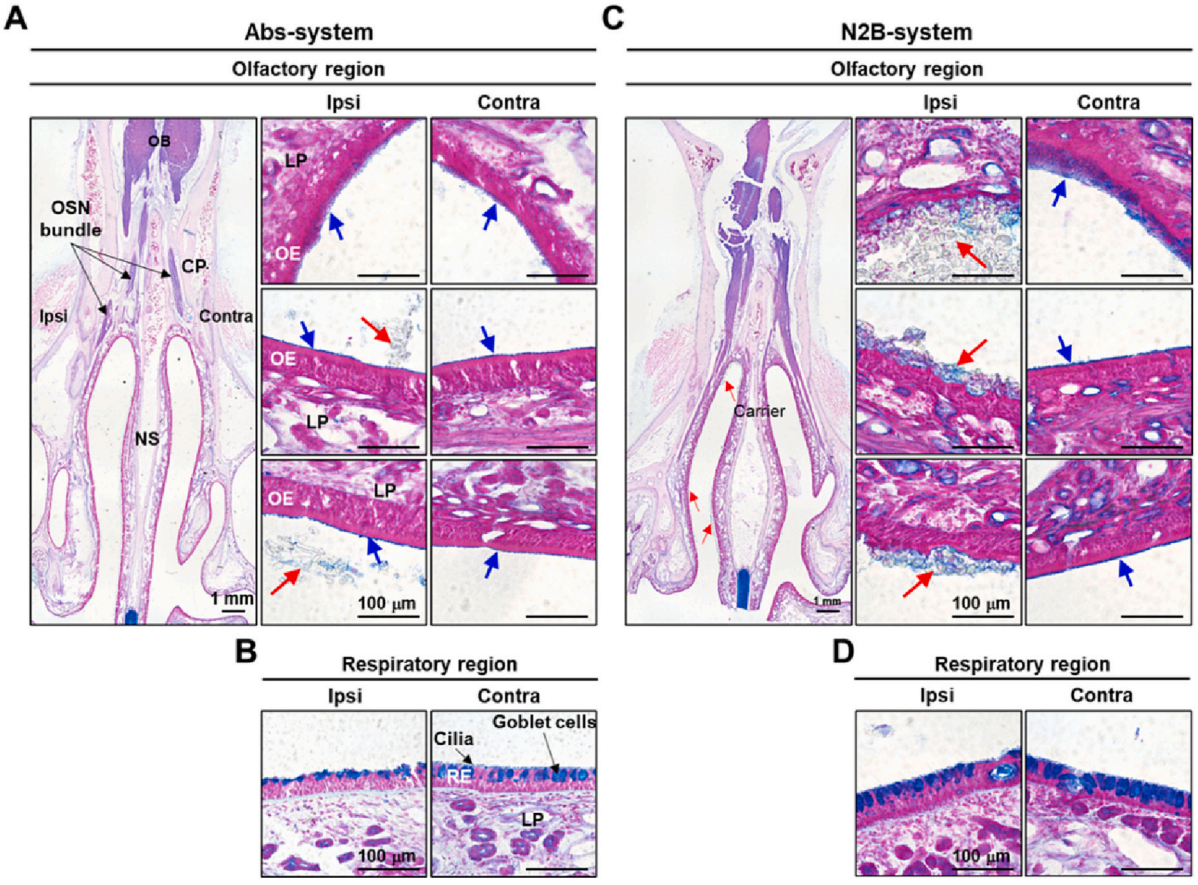

Fig. 4. Histological analysis of formulation deposition in the nasal cavity of cynomolgus monkeys ($n = 2$/group). Coronal sections of the nasal cavity were collected 30 min after IN administration. The 30 μm thick tissue sections were stained with Alcian blue/nuclear fast red solutions. (A) Carrier deposition in the olfactory region following administration using the Abs-system. (B) Carrier deposition in the respiratory region following administration using the Abs-system. (C) Carrier deposition in the olfactory region following administration using the N2B-system. (D) Carrier deposition in the respiratory region following administration using the N2B-system. Blue arrows indicate the mucus layer. Red arrows indicate the residual carrier on the nasal epithelium. OB, olfactory bulb; CP, cribriform plate; NS, nasal septum; OE, olfactory epithelium; LP, lamina propria; RE, respiratory epithelium. (For interpretation of the references to colour in this figure legend, the reader is referred to the web version of this article.)

changes were observed on the respiratory mucosa surface. In particular, the surface roughness and occasional cilia may have been caused by the transient adhesive effect of the carrier (Fig. 4B). In contrast, abundant carriers (red arrow) were observed for the N2B-system on the surface of the olfactory mucosa but not on the respiratory mucosa (Figs. 4C and D). Additionally, the carrier passed through mucus (blue arrow) and adhered directly to the surface of the olfactory epithelium. Moreover, to evaluate the time-dependent effects of mucociliary clearance on the adhesion and retention properties of the carrier in the olfactory mucosa using the N2B-system, the residual carrier (black arrow) deposition at 6 h after IN administration was compared with that at 30 min after IN administration. Fewer carriers were observed in the olfactory region at 6 h after IN administration than at 30 min after IN administration (Supplementary Figs. S1A and B). These results suggest that the carrier was eventually removed from the olfactory mucosa within 6 h of IN administration.

3.6. Localization of TR-DEX in monkey nasal cavity

To visualize the penetration behavior into the nasal epithelium, the formulation containing TR-DEX, which is a poorly permeable BBB agent [26], was administered intranasally into the right nostril using each of the systems. After 30 min of IN administration, the entire nasal cavity and olfactory bulb were isolated and divided into two blocks: the olfactory region with the olfactory bulb and the respiratory region (Fig. 5A). In the olfactory region, TR-DEX delivered by the Liquid-system was not observed in the olfactory epithelium. In contrast, TR-DEX delivered via the Abs-system was localized in the olfactory epithelial cell layer. Moreover, TR-DEX for the N2B-system was widely distributed in the olfactory epithelial cell layer and reached the lamina propria (Fig. 5B). In the respiratory region, TR-DEX delivered by the Abs-system was widely distributed from the respiratory epithelium cell layer to the lamina propria around the middle turbinate and the lateral wall of the nasal septum. In contrast, few TR-DEX signals were observed in the respiratory epithelial cells for both the Liquid-system and N2B-system (Fig. 5C). To investigate the N2B pathway of the TR-DEX delivered with the N2B-system, the olfactory region was immunostained with anti-OMP antibody and anti-fibronectin antibody as markers for the OSN bundles and extracellular matrix of the lamina propria, respectively [27]. Although no significant colocalization of TR-DEX (red) and OMP (green) was observed in the ipsilateral OSN bundles (Figs. 6A and B), TR-DEX appeared to penetrate the fibronectin-positive surrounding space (green) and the OSN bundles through cribriform foramina to the olfactory bulb (Fig. 6C).

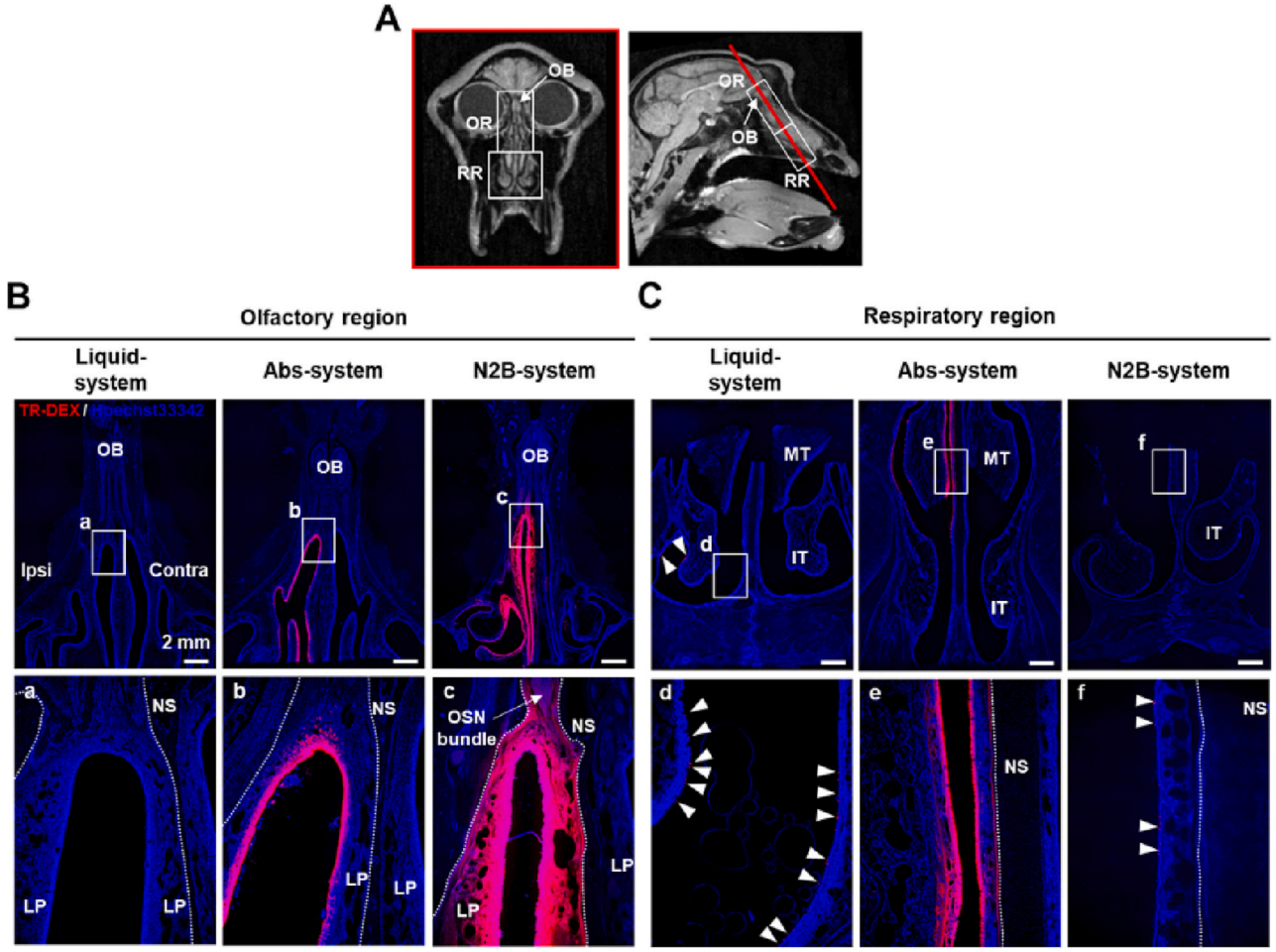

Fig. 5. Images of fluorescent signals from TR-DEX 30 min after IN administration using the three systems in cynomolgus monkeys (n = 2/group). (A) The exact coronal MRI image is indicated by the red line on the sagittal MRI image. The upper white box indicates the olfactory region of the bulb. The lower white box indicates the respiratory region. (B and C) Images of the coronal section showing TR-DEX fluorescence (red) in the olfactory region, including the olfactory bulb (B) and the respiratory region (C) 30 min after IN administration using each system. Low- and high-magnification images are shown in the upper and lower panels, respectively. White dashed lines represent the boundary between the lamina propria and bones. White arrowheads indicate scattered cellular uptake of TR-DEX in the respiratory epithelium. OB, olfactory bulb; NS, nasal septum; LP, lamina propria; OSN, olfactory sensory neuron; MT, middle turbinate; IT, inferior turbinate. (For interpretation of the references to colour in this figure legend, the reader is referred to the web version of this article.)

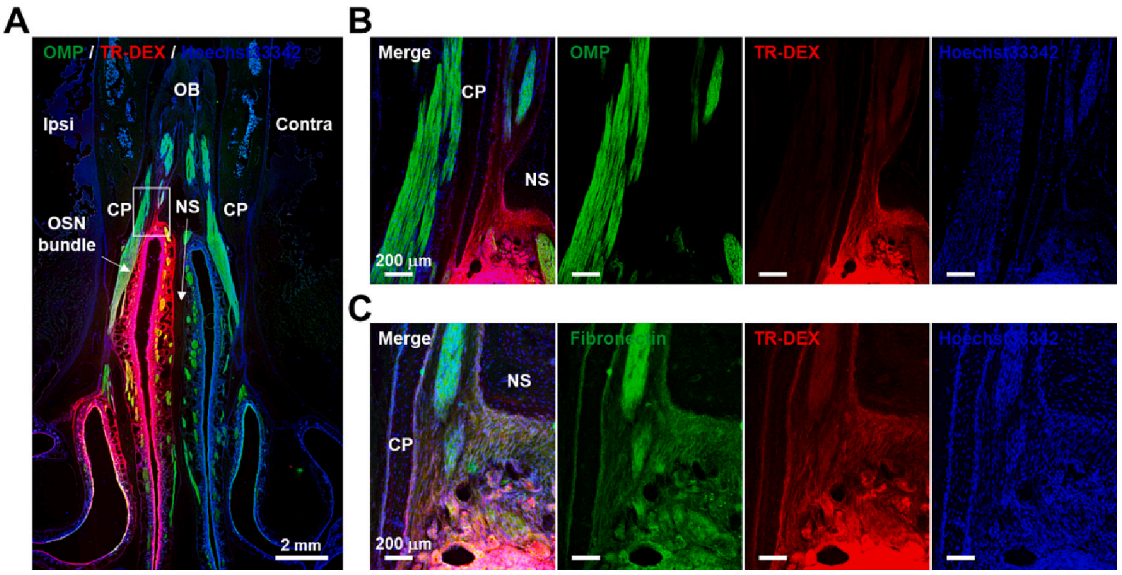

Fig. 6. Localization of TR-DEX in the olfactory region using the N2B-system at 30 min after IN administration (n = 2). (A) Fluorescence signals of TR-DEX (red) and OSN bundles (green) immunostained using an anti-olfactory marker protein (OMP) antibody were identified using fluorescence imaging. (B and C) High-magnification images were obtained from around the cribriform plate. (B) TR-DEX was detected along the OSN bundles (green) projecting lamina propria through cribriform foramina. (C) Lamina propria was identified using immunohistochemical staining with an anti-fibronectin (green) antibody. OB, olfactory bulb; CP, cribriform plate; NS nasal septum; OSN, olfactory sensory neuron. (For interpretation of the references to colour in this figure legend, the reader is referred to the web version of this article.)

3.7. Cellular uptakes of TR-DEX in nasal epithelial cells

The olfactory epithelial layer comprises at least five epithelial cell lineages: OSNs, sustentacular cells, basal cells, microvillar cells, and Bowman's gland cells. Ciliated, goblet, brush, and basal cells are the main cellular components of the respiratory epithelium [11]. The degree of selective cell-type uptake of TR-DEX in the olfactory epithelium was assessed by immunostaining the OSNs and sustentacular cells with anti-OMP and anti-CK18 antibodies, respectively [28]. The TR-DEX delivered with the N2B-system partially colocalized with the OMP-positive signals (green) in the middle layer of the olfactory epithelium (region surrounded by yellow dashed lines, Supplementary Fig. S2A). TR-DEX delivered with the N2B-system was abundantly detected in the upper half of the olfactory epithelium, which mainly expresses sustentacular cells (green, Supplementary Fig. S2B). Furthermore, the TR-DEX signal was only detected in the ipsilateral lamina propria but not in the contralateral lamina propria of the olfactory epithelium. To evaluate the possible involvement of the trigeminal route in delivering TR-DEX to the brain, an anti-PGP9.5 antibody was used to visualize the trigeminal nerves in the respiratory epithelium (Supplementary Fig. S3) [29]. The maxillary branch terminals of the trigeminal nerve reached the underlying basement membrane (region surrounded by yellow dashed lines) of the respiratory epithelium through the lamina propria. TR-DEX delivered with the N2B-system showed limited uptake by ciliated cells in the respiratory epithelium. In contrast, TR-DEX delivered with the Abs-system was abundantly observed in the respiratory epithelial layer and reached the underlying basement membrane through the lamina propria.

3.8. [^{18}F]Fallypride PET imaging after domperidone IN administration

Measurement of the percentage of receptor occupancy (*%RO*) is useful in investigating pharmaceutical efficacy, biodistribution, and visualizing drug deliverability to the brain in clinical and preclinical studies [30]. There are two methods to assess the *%RO*; first, to directly evaluate receptor binding of radiolabeled compounds after administration, and second, to indirectly evaluate receptor binding of non-radiolabeled model drugs by measuring radioligand displacement. In the current study, D2R competitive inhibition studies were performed using PET imaging with IV-administered [^{18}F]fallypride following domperidone IN administration to evaluate the possibility of domperidone delivery to the brain. Fig. 7A and B show the PET experimental schemes of the D2R competitive inhibition study for comparison among the three systems. Two additional doses were used for comparison among the three doses of domperidone delivered with the N2B-system. The specific uptake value–time profiles of [^{18}F]fallypride in each brain region following IN administration are shown in Supplementary Fig. S4. Representative transverse [^{18}F]fallypride PET/MRI images showing the caudate and putamen obtained from summed PET images 90–100 min after [^{18}F]fallypride administration are shown in Fig. 8A. The mean percentage of D2R occupancy (*%RO*) maps following IN domperidone administration are also shown in Fig. 8B. As is evident from the images, at a dose of 5 mg domperidone in the Liquid-system, the distribution patterns of radioactivity in the [^{18}F]fallypride images were similar to that of the control, and a low *%RO* was observed. In contrast, both the Abs-system and N2B-system demonstrated visible decreases in [^{18}F]fallypride accumulation in the caudate and putamen in the [^{18}F]fallypride images and subsequently increased in *%RO* compared with that of the Liquid-system (Figs. 8A and B). Comparing the three doses of domperidone with that of the N2B-system, [^{18}F]fallypride radioactivity in the caudate and putamen decreased with an increase in domperidone dosage, and the resulting *%RO* showed a dose-dependent increase following IN domperidone administration (Fig. 8B). The *%RO* of domperidone at a dose of 5 mg/nostril was calculated to estimate the differences in N2B domperidone delivery among the three systems (Fig. 9A). The *%RO* values for F. CTX, Cd, Pt, SN/VTA, and Thal for the N2B-system were significantly higher than those for the Liquid-system (F. CTX, $p = 0.0104$; Cd, $p = 0.0022$; Pt, $p = 0.0266$; SN/VTA, $p = 0.0184$ and Thal, $p = 0.0407$). The N2B-system also led to a marked increase in the *%RO* for F. CTX and Cd compared with the Abs-system (F. CTX, $p = 0.0157$ and Cd, $p = 0.0247$). Additionally, the effect of the three doses of domperidone in the N2B-system on *%RO* is shown in Fig. 9B. Upon comparing the results of the three doses of domperidone with that of the N2B-system, it was observed that the *%RO* for high-dose (15 mg) domperidone was significantly increased for all target regions compared with that of the low-dose (1.6 mg) domperidone (F. CTX, $p =$

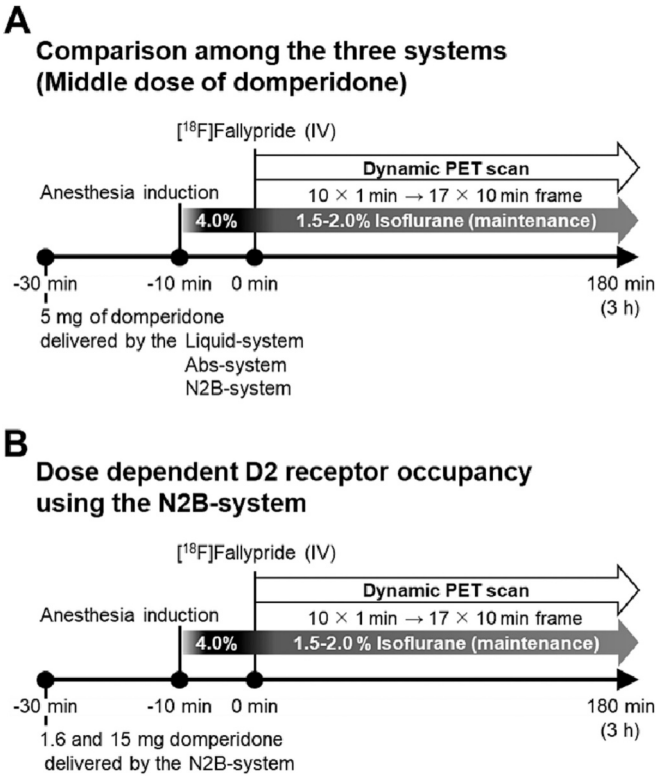

Fig. 7. Experimental design for [^{18}F]fallypride PET imaging with intranasally administered domperidone. The monkeys were initially anesthetized with 4% isoflurane 10 min before PET imaging. Thirty minutes after administering the domperidone dose, [^{18}F]fallypride was administered intravenously, followed immediately by a dynamic PET scan performed for 3 h (10 × 1 min/frame and subsequently 17 × 10 min/frame) under anesthesia with 1.5–2.0% isoflurane. (A) The three systems were compared based on a dose of 5 mg of domperidone/right nostril (middle dose, $n = 3$). (B) The N2B-system was compared at different doses of domperidone, namely, 1.6 and 15 mg of domperidone/right nostril (low and high doses, n = 3/group).

0.0132; Amy, $p = 0.0483$; Cd, $p = 0.0092$; Pt, $p = 0.0149$; GP, $p = 0.0168$; SN/VTA, $p = 0.0049$; Thal, $p = 0.0079$ and PAG, $p = 0.0096$). Notably, the high-dose (15 mg) domperidone showed a significantly higher *%RO* for Thal and PAG than that of the middle-dose (5 mg) domperidone (Thal, $p = 0.0441$ and PAG, $p = 0.0302$).

3.9. Plasma concentration of domperidone in PET study

During the PET imaging studies, blood was collected 30 min after IN administration to determine the plasma concentration of domperidone as an index of systemic absorption. The mean plasma concentrations of domperidone after administering at a dose of 5 mg domperidone using the Liquid-system, Abs-system, and N2B-system were 16.1 ± 8.17 ng/mL (n = 3), 42.1 ± 29.8 ng/mL (n = 3), and 46.0 ± 28.5 ng/mL (n = 3), respectively. Additionally, the mean plasma concentrations of domperidone after administering doses of 1.6 and 15 mg domperidone using the N2B-system were 29.6 ± 7.68 ng/mL (n = 3) and 84.8 ± 61.9 ng/mL (n = 3), respectively. The plasma concentrations of domperidone at the dose of 5 mg for both the Abs-system and N2B-system were higher (but not significantly higher) than that for the Liquid-system. This could be attributed to the difference in retention time of the formulation in the nasal mucosa. Domperidone exhibits significantly low oral bioavailability, primarily due to its rapid first-pass effect [31]. However, when administered intranasally, domperidone can circumvent the first-pass effect associated with liver and intestinal wall metabolism, consequently influencing nasal bioavailability. Nonetheless, in the Liquid-system, no Mn^{2+} signal was observed in the nasal cavity at any time point in the MEMRI study. Additionally, only a few TR-DEX signals were detected in the respiratory epithelial cells. These findings suggest that the liquid formulation delivered via the Liquid-system is rapidly eliminated from the nasal cavity, resulting in decreased plasma domperidone levels following IN administration. This decrease can be attributed to limited mucosal absorption compared to both the Abs-system and N2B-system. In contrast, both the Abs-system and N2B-system demonstrated Mn^{2+} signals in the nasal cavity at almost all time points in the MEMRI study, along with TR-DEX signals in the nasal mucosa 30 min after IN administration. These results indicate that both the Abs-system and N2B-system achieved rapid mucosal absorption through the combination of a highly mucoadhesive powder carrier and a dedicated nasal device, despite potential influence from mucosal clearance. Consequently, a greater amount of plasma domperidone is expected to be measured following IN administration with both the Abs-system and N2B-system compared to the Liquid-system. Furthermore, no significant difference was observed in the mean plasma concentration of domperidone at the dose of 5 mg between the Abs-system and N2B-system groups. The results of PET imaging showed that the N2B-system could lead to significantly increased *%RO* in the target brain regions such as F. CTX and Cd at the dose of 5 mg domperidone compared with those of the Abs-system. These results indicate the validity of more efficient direct N2B domperidone delivery resulting from olfactory region-selective IN administration using the N2B-system.

4. Discussion

To better understand the necessity of selective drug administration to the olfactory region for effective nasal drug delivery to the brain, the current study investigated the delivery characteristics, nasal distribution of formulations, and brain uptake of model drugs administered into the nasal cavity of cynomolgus monkeys for the N2B-system.

First, the delivery characteristics of the three systems were confirmed. The N2B-system showed significantly smaller ovality for spray pattern and shorter duration and peak times for plume intensity of the powder formulation than the Abs-system. In particular, the peak time of the plume intensity was the most differential parameter among the measured parameters concerning delivery characteristics. These differences in the plume intensity of the powder formulation between the N2B-system and Abs-system may be due to the differences in air pressure and supply air volume generated by each device. In addition, the delivery characteristics such as plume geometry, spray pattern, and the peak time of plume intensity and results of the secondary particle size (Dv50) studies for both the Abs-system and N2B-system exhibited narrower angle, smaller spray area, shorter peak times, and larger Dv50 than that of the Liquid-system. Thus, the significant differences in the delivery characteristics could be attributed to the formulation properties rather than device delivery characteristics.

The deliverability of the formulation to the olfactory region using each system was confirmed using a 3D-printed nasal cast of a cynomolgus monkey. For the N2B-system, the percentage of yellow dye distributed in the olfactory region was approximately 65%, which was significantly higher than that for the Abs-system and the Liquid-system. Thus, the N2B-system achieved more efficient formulation delivery to the olfactory region. In particular, achieving efficient delivery of the powder formulation through the narrow nasal cavity to the respiratory and olfactory regions requires specific delivery characteristics, such as a narrow angle and small spray area. These factors significantly influence the distribution of the nasal formulation, ensuring optimal coverage. Furthermore, it has been suggested that the appropriate air pressure settings for formulation injection, which affect the short plume intensity, play a crucial role in selectively delivering the powder formulation to the olfactory region located in the innermost part and roof of the nasal cavity.

The nasal mucosa (including that of the respiratory and olfactory epithelium) in living animals has a mucociliary clearance to protect the

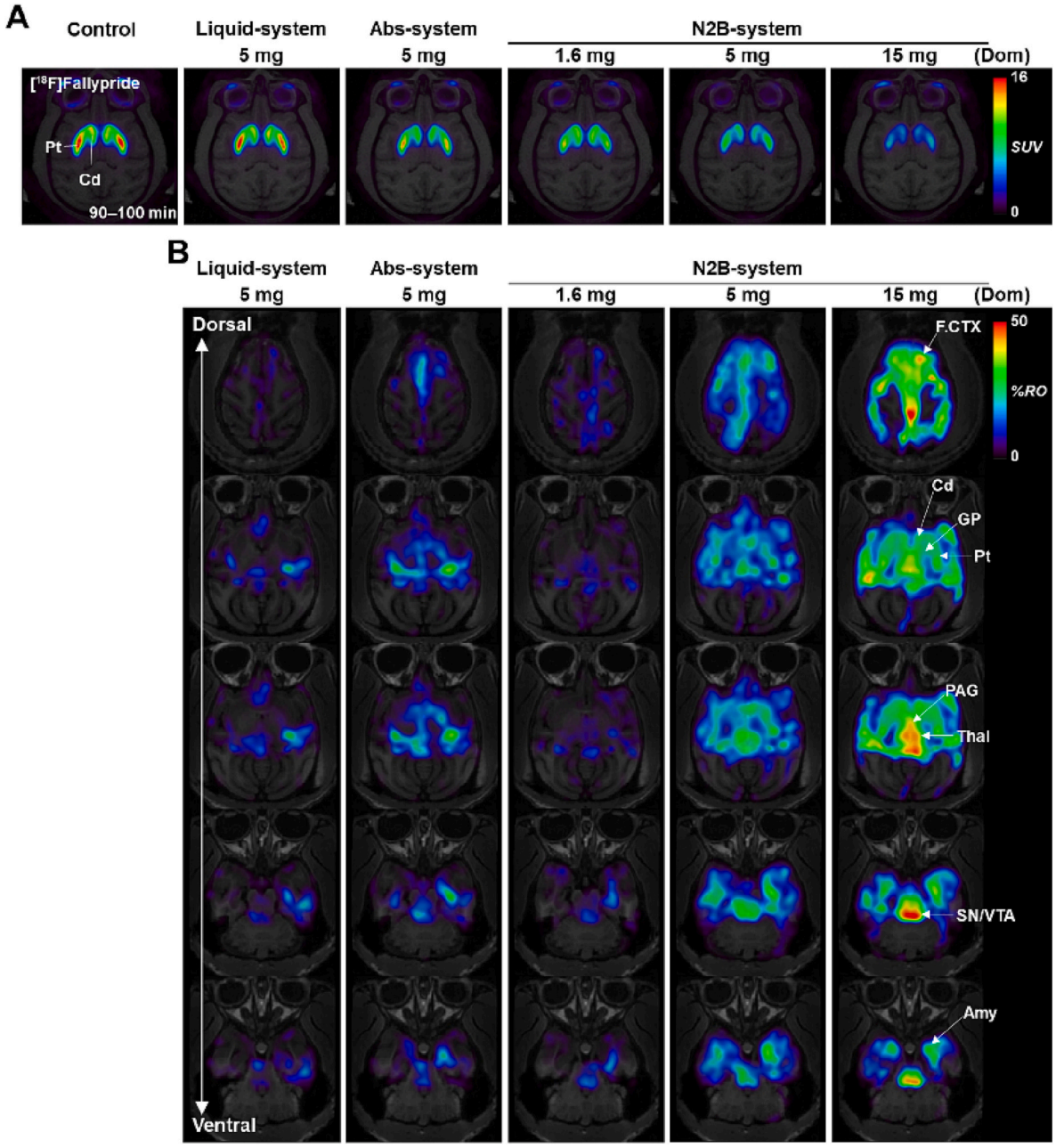

Fig. 8. (A) The representative transverse images are [^{18}F]Fallypride PET images. All PET images were fused with the MRI images to identify the brain regions. [^{18}F]Fallypride PET images showing caudate and putamen were obtained from summed PET images at 90–100 min after [^{18}F]fallypride administration. (B) The mean *%RO* maps were generated to visually compare the difference among each experimental group using the PNEURO tool ($n = 3$/group). Cd, caudate; Pt, putamen; F.CTX, frontal cortex; GP, globus pallidus; PAG, periaqueductal gray; Thal, thalamus; SN/VTA, substantia nigra/ventral tegmental area; Amy, amygdala; Dom, domperidone; SUV, standardized uptake value; and *%RO*, percent of receptor occupancy.

airway from inhaled infectants, pollutants, particulates [32], and medicinal substances [33], making it difficult for direct translation of the results of the formulation distribution in the 3D-printed nasal cast to living animals. In this study, MEMRI, which uses a formulation containing manganese chloride as a positive contrast agent, was used to confirm the nasal formulation distribution in living monkeys. Similar to the results of the distribution study using the 3D-printed nasal cast, the N2B-system was confirmed to have the highest distribution of Mn^{2+} in the olfactory region (Fig. 3A). Despite the absence of a carrier on the surface of the respiratory mucosa for the Abs-system at 30 min after IN administration during the histological assessment, there was a consistent detection of the Mn^{2+} signal in the respiratory region throughout almost all time points. Furthermore, fluorescence imaging revealed the distribution of TR-DEX, delivered by the Abs-system, from the respiratory epithelial cell layer to the lamina propria at 30 min, without any residual carriers observed on the surface of the respiratory epithelium. These findings strongly suggest the possibility that the IN-administered Mn^{2+} and TR-DEX, delivered by the Abs-system, were rapidly taken up into the respiratory epithelial cells and/or trigeminal nerve fibers located in the lamina propria of the respiratory region prior to being influenced by the carrier's interaction with mucociliary clearance.

Additionally, the Mn^{2+} signal was observed for up to 24 h after IN administration in the olfactory region of the nasal cavity for the N2B-system (Fig. 3A). Moreover, histological assessment using Alcian blue/nuclear fast red staining showed that a carrier consisting of the powder formulation was clearly observed in the olfactory mucosa 30 min after

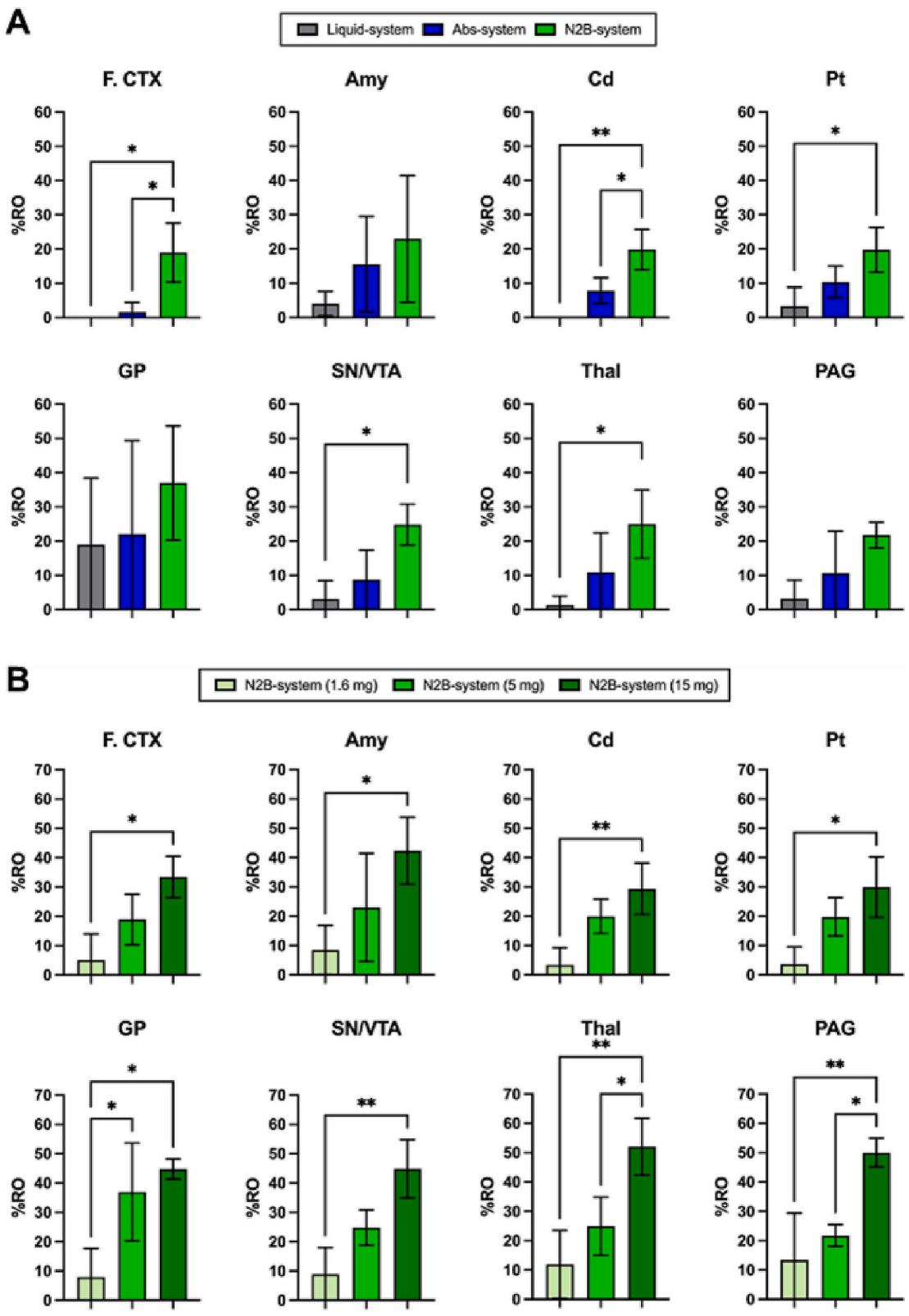

Fig. 9. Brain regional D2R occupancy (*RO*) of domperidone as revealed using [^{18}F]fallypride PET imaging. (A) The percentage of *RO* (*%RO*) obtained from the comparison study for the three systems is shown in each target region (* $p < 0.05$, ** $p < 0.01$). Data are presented as mean ± SD ($n = 3$). (B) The *%RO* obtained from the comparison study for the N2B-system with different doses of domperidone are shown for each target region (* $p < 0.05$, ** $p < 0.01$). Data are presented as mean ± SD (n = 3). The target regions were F.CTX, frontal cortex; Cd, caudate; Pt, putamen; Amy, amygdala; GP, globus pallidus; SN/VTA, substantia nigra/ventral tegmental area; Thal, thalamus; and PAG, periaqueductal gray. The cerebellum was set as a reference region.

administration using the N2B-system (Fig. 4C). These in vitro and in vivo nasal distribution studies suggest that the N2B-system is effective in increasing the distribution of the powder formulations in the olfactory region, and the nasal retention time may have been prolonged by the possible combined effect of highly pressurized air, supply air volume, and high mucoadhesive property of the nasal powder formulation. Moreover, using the N2B-system resulted in marked Mn^{2+} accumulation in the ipsilateral olfactory bulb owing to the highly selective formulation distribution and prolonged retention of Mn^{2+} in the olfactory region (Figs. 3B, C). These results also suggest that the N2B-system effectively delivers medicines and diagnostic drugs to OSNs in the olfactory region. Olfacto-scintigraphy, in particular, may be beneficial for diagnosing olfactory function by employing the radioisotope Thallium-201 as a safety tracer to examine the olfactory nerve route and migration to the olfactory bulb [34]. However, human subjects must restrict their body movement after IN administration to minimize spills from the liquid formulation from the olfactory region to the external nostril or nasopharynx [35]. In the case mentioned above, the N2B-system containing Thallium-201 was expected to relieve the restraint of behavioral restrictions during diagnosis.

Although MEMRI imaging is useful for detecting the nasal deposition of formulations and for olfactory tract imaging, it has a resolution limit for visualizing the fine structure related to the N2B drug delivery pathway, such as in the paracellular and transcellular routes and the direct transport of drugs to the brain via the perivascular spaces [11]. Fluorescence imaging was performed to visualize the N2B pathway using TR-DEX. Fluorophore-conjugated dextran, including TR-DEX, is often used as a model drug in N2B drug delivery research [26]. Following IN administration, dextran distribution was observed to reach the olfactory bulb along the OSN bundles crossing the cribriform plate via the olfactory epithelium and underlying lamina propria [36]. In the present study, nasal localization of TR-DEX was observed 30 min after IN administration in the nasal cavity of cynomolgus monkeys for all three systems. For the N2B-system, but not the other systems, abundant TR-DEX was localized mainly in the sustentacular cells and showed a gradual decrease from the apical to the basal side to the lamina propria of the olfactory epithelium in the olfactory region. These results suggest that the principal N2B delivery pathway for TR-DEX is a composite of the transcellular route via sustentacular cells and paracellular diffusion across the intercellular space in the olfactory region. Thus, concentration gradient diffusion plays an important role in the direct N2B delivery of the non-directional tracer TR-DEX.

In contrast, the trigeminal route has also been investigated as a potential transport route for substances from nasal epithelium to the brain [37]. The respiratory region is innervated by the maxillary branch terminals of the trigeminal nerve, which originally project from the brainstem. Additionally, the olfactory region is innervated by the nasociliary nerve, which is an intermediate branch of the ophthalmic division of the trigeminal nerve through the cribriform plate [38]. The fluorescent signal of TR-DEX for the Abs-system but not for the N2B-system, was observed in the respiratory epithelium and underlying lamina propria, which are innervated by the trigeminal nerve as pan-neuronal marker PGP9.5-positive filaments (Supplementary Fig. S3). However, this result did not comply with the immunohistological assessment of TR-DEX uptake along the trigeminal route, such as in the trigeminal ganglion and pons. These results suggest the possible involvement of the trigeminal route of the respiratory region and its contribution to transport via the respiratory epithelium to deliver TR-DEX and other substances to the brain. In the current study, whether the contribution of the trigeminal route through the nasociliary nerve leads to nasal drug delivery to the brain on the olfactory region remains unclear and should be addressed in further studies.

As TR-DEX could not accumulate in a specific brain region, identifying TR-DEX uptake in the brain parenchyma, except in the olfactory bulb, 30 min after IN administration was challenging. In our previous study, we used nuclear imaging with radiopharmaceutical [^{123}I] iodobenzamide (IBZM), which is a D2R ligand with high BBB permeability, to indirectly evaluate brain uptake of IN-administered domperidone, which has poor BBB permeability [8]. Increasing *%RO* of domperidone caused by competition with D2R-[^{123}I]IBZM binding was confirmed in the striatum following IN administration, suggesting that indirect nuclear imaging would be useful for assessing IN-administrated drug delivery to the brain.

In the present study, the *%RO* of IN-administered domperidone was evaluated in cynomolgus monkeys using PET imaging with intravenously administered [^{18}F]fallypride as an indicator for comparison of the three systems [39]. The VOI of the target regions was preset on highly D2R-expressing brain regions such as F. CTX, Amy, Cd, Pt, GP, SN/VTA, Thal, and PAG [40]. The N2B-system showed a markedly higher *%RO* in F. CTX and Cd than the Abs-system. Simultaneously, the N2B-system also showed significantly higher *%RO* in F. CTX, Cd, Pt, SN/VTA, and Thal than did the Liquid-system. Moreover, for the N2B-system, a dose-dependent increase in *%RO* was observed in all target regions when comparing low and high doses of domperidone.

F. CTX, Cd, Pt, SN/VTA, and Thal showed higher *%RO* for the N2B-system among the three systems involved in the central dopaminergic system [41]. The nigrostriatal pathway has dopaminergic projections from the SN to the Cd and Pt, and abnormalities in this pathway cause motor dysfunction [42,43]. The mesocortical pathway also contributes to dopamine transmission from the VTA to F. CTX, and dysfunction of this pathway causes cognitive and emotional impairment. Moreover, Amy, GP, and PAG showed increased *%RO* with increasing dosage of IN domperidone administered using the N2B-system. These regional dopaminergic functions are involved in impulsive behavior, voluntary movement, and modulation of nociception [44–46]. These findings suggest that the N2B-system is expected to contribute to pharmaceutical interventions for several types of CNS disorders caused by dopaminergic dysregulation.

The effects of IV administration of domperidone on *%RO* in cynomolgus monkeys were also determined to estimate the delivery of domperidone to the brain from the systemic circulation across the BBB (data not shown). However, a monkey that received an IV dose of 5 mg domperidone experienced sudden death owing to the adverse effects of domperidone. Serious side effects of IV domperidone include cardiac arrhythmias accompanied by QT interval prolongation, leading to sudden death in humans [47]. Abnormal clinical signs such as sedation and somnolence have been observed for 1–5 mg doses of IV domperidone. Additionally, in the preliminary PET imaging study that was conducted to estimate the effect of an IV dose of 1 mg domperidone in a cynomolgus monkey, no notable changes were observed in the BP_{ND} and *%RO* in the caudate and putamen regions compared with that of the control. Therefore, further experiments with the proposed increase in the number of animals were discontinued from the perspective of animal ethics. Notably, IN domperidone delivered with all three systems showed no behavioral abnormalities at any domperidone dosage, suggesting that nasal drug delivery reduces systemic adverse reactions. Furthermore, although no significant difference was observed in the plasma domperidone levels between the Abs-system and N2B-system, the N2B-system did achieve efficient N2B drug delivery irrespective of domperidone delivery from the systemic circulation.

In the present study, the potential for efficient nasal drug delivery to the brain by targeting the olfactory region was achieved with the N2B-system, comprising a highly mucoadhesive powder carrier and a newly developed N2B device. The N2B-system showed a dominant formulation distribution in the olfactory region in both the in vitro experiment using a 3D-printed nasal cast and in vivo experiment using MEMRI. Additionally, the N2B-system exhibited a possible N2B delivery pathway of composite routes crossing the cribriform plate via the olfactory epithelium and underlying lamina propria on MEMRI and fluorescence imaging. Moreover, PET imaging showed the highest *%RO* of domperidone delivered by the N2B-system in several brain regions compared with that of the other systems, suggesting that the olfactory region is a suitable

target for efficient N2B drug delivery in cynomolgus monkeys. In contrast, the Abs-system showed a slight decrease in BP_{ND} and an increase in *%RO* compared with that of the control group owing to the possible effect of domperidone uptake by the brain caused by a small amount of IN formulation delivery to the olfactory region. These results suggest that the additional involvement of the trigeminal route could play a partial role in nasal drug delivery to the brain. Further experiments are necessary to clarify the mechanism underlying drug transport into the brain via the trigeminal route in the olfactory and/or respiratory regions. Although the comparison between the N2B-system and Abs-system at the same dose of domperidone indicated that the olfactory region-selective formulation distribution was efficient for N2B drug delivery, the contributing factors remain unclear with regard to drug delivery to specific brain regions, such as formulation distribution ratio and pattern of the olfactory region compared with that of the respiratory region in the nasal cavity associated with the consumed formulation quantity for IN administration. To further evaluate the importance of olfactory region-selective drug distribution, the dose-dependency in *% RO* of domperidone via the respiratory region needs to be evaluated to confirm whether brain uptake of the drug comparable to that observed with the N2B-system can be achieved. Additionally, to enhance our understanding of N2B delivery, it is recommended to employ *ex vivo* nuclear imaging like single-photon emission computerized tomography (SPECT) imaging or autoradiography in future studies. These techniques employ radiolabeled compounds with nuclides that have longer radioactive half-lives. Through these studies, direct evidence can be obtained concerning the delivery of drugs from the nasal cavity to the brain (N2B delivery), providing a detailed understanding of their uptake profile in the brain. Besides the potential application of the N2B-system for delivering P-gp substrates such as domperidone to the brain, further investigations are necessary to determine the efficacy of the N2B-system in delivering other drug types expected to improve brain delivery, including oligonucleotide therapeutics, antibodies, peptides, and nanoparticles. This exploration represents an important step in assessing the versatility and effectiveness of the N2B-system for diverse drug classes. Furthermore, the results obtained from the current experiments should be extrapolated to facilitate the development and optimization of N2B drug delivery systems for clinical applications. This extrapolation will play a vital role in translating the findings into practical solutions that can be effectively implemented in a clinical setting, thereby enhancing the potential of N2B drug delivery for therapeutic purposes.

5. Conclusion

This study demonstrated that the olfactory region is a suitable target for efficient nasal drug delivery to the brain in cynomolgus monkeys, which have similar nasal anatomy to humans. Furthermore, using the N2B-system, consisting of a highly mucoadhesive powder carrier and a newly designated N2B device with optimized delivery characteristics is an adequate approach for promoting N2B drug delivery research and developing an effective technology for nasal drug delivery to the brain in humans.

Disclosure statement

Suzuki C and Magata Y have no conflicts of interest to disclose. Sasaki K, Fukakusa S, Torikai Y, Sonohata I, Kawahata T, and Haruta S are full-time employees of Shin Nippon Biomedical Laboratories, Ltd. (SNBL). Kawai K is a scientific adviser for SNBL.

Compliance with ethical standards

All animal experiments, except for the PET imaging study, were conducted with the approval of the Institutional Animal Care and Use Committee of Shin Nippon Biomedical Laboratories, Ltd. (Approval No. IACUC996–204, −229, and − 233), which is fully AAALAC-certified. The PET imaging study was performed in accordance with the institutional and national guidelines regarding animal care and was approved by the Animal Care and Use Committee of the Hamamatsu University School of Medicine (Approval No. 2019040).

Funding

This study was funded by SNBL. The company had no role in the design of the study, collection, analyses, interpretation of data, writing of the manuscript, or decision to publish the results.

CRediT authorship contribution statement

Keita Sasaki: Conceptualization, Formal analysis, Investigation, Methodology, Validation, Visualization, Writing – original draft, Writing – review & editing, Data curation, Project administration. **Shota Fukakusa:** Formal analysis, Investigation, Methodology, Validation, Visualization, Writing – review & editing, Data curation. **Yusuke Torikai:** Conceptualization, Investigation, Methodology, Writing – review & editing. **Chie Suzuki:** Formal analysis, Investigation, Methodology, Validation, Visualization, Writing – original draft, Writing – review & editing. **Ikumi Sonohata:** Formal analysis, Methodology, Writing – review & editing. **Takuto Kawahata:** Investigation, Methodology, Writing – review & editing. **Yasuhiro Magata:** Investigation, Methodology, Validation, Visualization, Writing – review & editing. **Keiichi Kawai:** Methodology, Writing – review & editing. **Shunji Haruta:** Conceptualization, Funding acquisition, Methodology, Project administration, Writing – original draft, Writing – review & editing.

Data availability

The authors confirm that data supporting the findings of this study are available within the article.

Acknowledgments

All studies were conducted at Shin Nippon Biomedical Laboratories, Ltd., and Hamamatsu University School of Medicine. We are thankful to Mr. Akifumi Kyuno, Ms. Nami Yasuda, Mr. Sawato Kawamura, and Mr. Shinji Nishizono of Shin Nippon Biomedical Laboratories, Ltd., for providing expertise that greatly assisted the research. We thank the research members of the Laboratory Animal Facilities & Services and Promotion Center for Medical Collaboration & Intellectual Property, Hamamatsu University School of Medicine.

Appendix A. Supplementary data

Supplementary data to this article can be found online at https://doi.org/10.1016/j.jconrel.2023.06.005.

References

[1] H. Kadry, B. Noorani, L. Cucullo, A blood-brain barrier overview on structure, function, impairment, and biomarkers of integrity, Fluids Barriers CNS. 17 (2020) 69, https://doi.org/10.1186/s12987-020-00230-3.
[2] R. Cecchelli, V. Berezowski, S. Lundquist, M. Culot, M. Renftel, M.P. Dehouck, L. Fenart, Modelling of the blood-brain barrier in drug discovery and development, Nat. Rev. Drug Discov. 6 (2007) 650–661, https://doi.org/10.1038/nrd2368.
[3] W. Alabsi, B.B. Eedara, D. Encinas-Basurto, R. Polt, H.M. Mansour, Nose-to-brain delivery of therapeutic peptides as nasal aerosols, Pharmaceutics. 14 (2022), https://doi.org/10.3390/pharmaceutics14091870.
[4] N.N. Kumar, J.J. Lochhead, M.E. Pizzo, G. Nehra, S. Boroumand, G. Greene, R. G. Thorne, Delivery of immunoglobulin G antibodies to the rat nervous system following intranasal administration: distribution, dose-response, and mechanisms of delivery, J. Control. Release 286 (2018) 467–484, https://doi.org/10.1016/j.jconrel.2018.08.006.
[5] M. Milewski, A. Goodey, D. Lee, E. Rimmer, R. Saklatvala, S. Koyama, M. Iwashima, S. Haruta, Rapid absorption of dry-powder intranasal oxytocin, Pharm. Res. 33 (2016) 1936–1944, https://doi.org/10.1007/s11095-016-1929-x.

[6] D. Alarcón-Arís, R. Pavia-Collado, L. Miquel-Rio, V. Coppola-Segovia, A. Ferrés-Coy, E. Ruiz-Bronchal, M. Galofré, V. Paz, L. Campa, R. Revilla, A. Montefeltro, J. H. Kordower, M. Vila, F. Artigas, A. Bortolozzi, Anti-alpha-synuclein ASO delivered to monoamine neurons prevents alpha-synuclein accumulation in a Parkinson's disease-like mouse model and in monkeys, EBiomedicine. 59 (2020), 102944, https://doi.org/10.1016/j.ebiom.2020.102944.
[7] L.A. Bors, Á. Bajza, M. Mándoki, B.J. Tasi, G. Cserey, T. Imre, P. Szabó, F. Erdő, Modulation of nose-to-brain delivery of a P-glycoprotein (MDR1) substrate model drug (quinidine) in rats, Brain Res. Bull. 160 (2020) 65–73, https://doi.org/10.1016/j.brainresbull.2020.04.012.
[8] A. Mizutani, M. Kobayashi, M. Ohuchi, K. Sasaki, Y. Muranaka, Y. Torikai, S. Fukakusa, C. Suzuki, R. Nishii, S. Haruta, Y. Magata, K. Kawai, Indirect SPECT imaging evaluation for possible nose-to-brain drug delivery using a compound with poor blood-brain barrier permeability in mice, Pharmaceutics. 14 (2022), https://doi.org/10.3390/pharmaceutics14051026.
[9] H. Goel, V. Kalra, S.K. Verma, S.K. Dubey, A.K. Tiwary, Convolutions in the rendition of nose to brain therapeutics from bench to bedside: feats & fallacies, J. Control. Release 341 (2022) 782–811, https://doi.org/10.1016/j.jconrel.2021.12.009.
[10] L.R. Hanson, W.H. Frey 2nd, Intranasal delivery bypasses the blood-brain barrier to target therapeutic agents to the central nervous system and treat neurodegenerative disease, BMC Neurosci. 9 (Suppl. 3) (2008) S5, https://doi.org/10.1186/1471-2202-9-S3-S5.
[11] J.J. Lochhead, R.G. Thorne, Intranasal delivery of biologics to the central nervous system, Adv. Drug Deliv. Rev. 64 (2012) 614–628, https://doi.org/10.1016/j.addr.2011.11.002.
[12] C.V. Pardeshi, V.S. Belgamwar, Direct nose to brain drug delivery via integrated nerve pathways bypassing the blood-brain barrier: an excellent platform for brain targeting, Expert Opin. Drug Deliv. 10 (2013) 957–972, https://doi.org/10.1517/17425247.2013.790887.
[13] M. Fukuda, T. Kanazawa, S. Iioka, T. Oguma, R. Iwasa, S. Masuoka, N. Suzuki, Y. Kosuge, T. Suzuki, Quantitative analysis of inulin distribution in the brain focused on nose-to-brain route via olfactory epithelium by reverse esophageal cannulation, J. Control. Release 332 (2021) 493–501, https://doi.org/10.1016/j.jconrel.2021.02.024.
[14] F. Maigler, S. Ladel, J. Flamm, S. Gänger, B. Kurpiers, S. Kiderlen, R. Völk, C. Hamp, S. Hartung, S. Spiegel, A. Soleimanizadeh, K. Eberle, R. Hermann, L. Krainer, C. Pitzer, K. Schindowski, Selective CNS targeting and distribution with a refined region-specific intranasal delivery technique via the olfactory mucosa, Pharmaceutics. 13 (2021), https://doi.org/10.3390/pharmaceutics13111904.
[15] L.A. Keller, O. Merkel, A. Popp, Intranasal drug delivery: opportunities and toxicologic challenges during drug development, Drug Deliv. Transl. Res. 12 (2022) 735–757, https://doi.org/10.1007/s13346-020-00891-5.
[16] R. Chamanza, J.A. Wright, A review of the comparative anatomy, histology, physiology and pathology of the nasal cavity of rats, mice, dogs and non-human primates. Relevance to inhalation toxicology and human health risk assessment, J. Comp. Pathol. 153 (2015) 287–314, https://doi.org/10.1016/j.jcpa.2015.08.009.
[17] J.R. Harkema, Comparative aspects of nasal airway anatomy: relevance to inhalation toxicology, Toxicol. Pathol. 19 (1991) 321–336, https://doi.org/10.1177/019262339101900402.
[18] Y. Torikai, Y. Sasaki, K. Sasaki, A. Kyuno, S. Haruta, A. Tanimoto, Evaluation of systemic and mucosal immune responses induced by a nasal powder delivery system in conjunction with an OVA antigen in cynomolgus monkeys, J. Pharm. Sci. 110 (2021) 2038–2046, https://doi.org/10.1016/j.xphs.2020.11.023.
[19] I. Ieiri, Functional significance of genetic polymorphisms in P-glycoprotein (MDR1, ABCB1) and breast cancer resistance protein (BCRP, ABCG2), Drug Metab. Pharmacokinet. 27 (2012) 85–105, https://doi.org/10.2133/dmpk.dmpk-11-rv-098.
[20] A.H. Schinkel, E. Wagenaar, C.A. Mol, L. van Deemter, P-glycoprotein in the blood-brain barrier of mice influences the brain penetration and pharmacological activity of many drugs, J. Clin. Invest. 97 (1996) 2517–2524, https://doi.org/10.1172/JCI118699.
[21] B.S. Moon, J.H. Park, H.J. Lee, J.S. Kim, H.S. Kil, B.S. Lee, D.Y. Chi, B.C. Lee, Y. K. Kim, S.E. Kim, Highly efficient production of [(18)F]fallypride using small amounts of base concentration, Appl. Radiat. Isot. 68 (2010) 2279–2284, https://doi.org/10.1016/j.apradiso.2010.06.016.
[22] M. Watanabe, A. Saito, T. Isobe, K. Ote, R. Yamada, T. Moriya, T. Omura, Performance evaluation of a high-resolution brain PET scanner using four-layer MPPC DOI detectors, Phys. Med. Biol. 62 (2017) 7148–7166, https://doi.org/10.1088/1361-6560/aa82e8.
[23] J. Logan, J.S. Fowler, N.D. Volkow, G.J. Wang, Y.S. Ding, D.L. Alexoff, Distribution volume ratios without blood sampling from graphical analysis of PET data, J. Cereb. Blood Flow Metab. 16 (1996) 834–840, https://doi.org/10.1097/00004647-199609000-00008.
[24] Z. Fa, P. Zhang, F. Huang, P. Li, R. Zhang, R. Xu, Z. Wen, X. Jiang, Activity-induced manganese-dependent functional MRI of the rat visual cortex following intranasal manganese chloride administration, Neurosci. Lett. 481 (2010) 110–114, https://doi.org/10.1016/j.neulet.2010.06.063.
[25] C.A. Massaad, R.G. Pautler, Manganese-enhanced magnetic resonance imaging (MEMRI), Methods Mol. Biol. 711 (2011) 145–174, https://doi.org/10.1007/978-1-61737-992-5_7.
[26] J.J. Lochhead, D.J. Wolak, M.E. Pizzo, R.G. Thorne, Rapid transport within cerebral perivascular spaces underlies widespread tracer distribution in the brain after intranasal administration, J. Cereb. Blood Flow Metab. 35 (2015) 371–381, https://doi.org/10.1038/jcbfm.2014.215.
[27] T. Tanos, A.M. Saibene, C. Pipolo, P. Battaglia, G. Felisati, A. Rubio, Isolation of putative stem cells present in human adult olfactory mucosa, PLoS One 12 (2017), e0181151, https://doi.org/10.1371/journal.pone.0181151.
[28] B. Bryche, A. St Albin, S. Murri, S. Lacôte, C. Pulido, M. Ar Gouilh, S. Lesellier, A. Servat, M. Wasniewski, E. Picard-Meyer, E. Monchatre-Leroy, R. Volmer, O. Rampin, R. Le Goffic, P. Marianneau, N. Meunier, Massive transient damage of the olfactory epithelium associated with infection of sustentacular cells by SARS-CoV-2 in golden Syrian hamsters, Brain Behav. Immun. 89 (2020) 579–586, https://doi.org/10.1016/j.bbi.2020.06.032.
[29] H. Nishijima, K. Kondo, M. Toma-Hirano, S. Iwasaki, S. Kikuta, C. Fujimoto, R. Ueha, R. Kagoya, T. Yamasoba, Denervation of nasal mucosa induced by posterior nasal neurectomy suppresses nasal secretion, not hypersensitivity, in an allergic rhinitis rat model, Lab. Investig. 96 (2016) 981–993, https://doi.org/10.1038/labinvest.2016.72.
[30] A. Takano, A. Varrone, B. Gulyas, P. Salvadori, A. Gee, A. Windhorst, J. Vercouillie, G. Bormans, A.A. Lammertsma, C. Halldin, Guidelines to PET measurements of the target occupancy in the brain for drug development, Eur. J. Nucl. Med. Mol. Imaging 43 (2016) 2255–2262, https://doi.org/10.1007/s00259-016-3476-4.
[31] B.L. Athukuri, P. Neerati, Enhanced Oral bioavailability of Domperidone with Piperine in male Wistar rats: involvement of CYP3A1 and P-gp inhibition, J. Pharm. Pharm. Sci. 20 (2017) 28–37, https://doi.org/10.18433/J3MK72.
[32] L.E. Kuek, R.J. Lee, First contact: the role of respiratory cilia in host-pathogen interactions in the airways, Am. J. Physiol. Lung Cell Mol. Physiol. 319 (2020) L603–L619, https://doi.org/10.1152/ajplung.00283.2020.
[33] J. Jiao, L. Zhang, Influence of intranasal drugs on human nasal mucociliary clearance and ciliary beat frequency, allergy asthma, Immunol. Res. 11 (2019) 306–319, https://doi.org/10.4168/aair.2019.11.3.306.
[34] H. Shiga, K. Washiyama, K. Hirota, R. Amano, M. Furukawa, T. Miwa, Use of thallium transport to visualize functional olfactory nerve regeneration in vivo, Rhinology 47 (2009) 460–464, https://doi.org/10.4193/Rhin08.213.
[35] H. Shiga, J. Taki, K. Washiyama, J. Yamamoto, S. Kinase, K. Okuda, S. Kinuya, N. Watanabe, H. Tonami, K. Koshida, R. Amano, M. Furukawa, T. Miwa, Assessment of olfactory nerve by SPECT-MRI image with nasal thallium-201 administration in patients with olfactory impairments in comparison to healthy volunteers, PLoS One 8 (2013), e57671, https://doi.org/10.1371/journal.pone.0057671.
[36] B. Jansson, E. Björk, Visualization of in vivo olfactory uptake and transfer using fluorescein dextran, J. Drug Target. 10 (2002) 379–386, https://doi.org/10.1080/1061186021000001823.
[37] Y. Li, C. Wang, S. Zong, J. Qi, X. Dong, W. Zhao, W. Wu, Q. Fu, Y. Lu, Z. Chen, The trigeminal pathway dominates the nose-to-brain transportation of intact polymeric nanoparticles: evidence from aggregation-caused quenching probes, J. Biomed. Nanotechnol. 15 (2019) 686–702, https://doi.org/10.1166/jbn.2019.2724.
[38] T.G. White, K. Powell, K.A. Shah, H.H. Woo, R.K. Narayan, C. Li, Trigeminal nerve control of cerebral blood flow: a brief review, Front. Neurosci. 15 (2021), 649910, https://doi.org/10.3389/fnins.2021.649910.
[39] J. Mukherjee, B.T. Christian, T.K. Narayanan, B. Shi, J. Mantil, Evaluation of dopamine D-2 receptor occupancy by clozapine, risperidone, and haloperidol in vivo in the rodent and nonhuman primate brain using 18F-fallypride, Neuropsychopharmacology 25 (2001) 476–488, https://doi.org/10.1016/S0893-133X(01)00251-2.
[40] K.L. Seaman, C.T. Smith, E.J. Juarez, L.C. Dang, J.J. Castrellon, L.L. Burgess, M. D. San Juan, P.M. Kundzicz, R.L. Cowan, D.H. Zald, G.R. Samanez-Larkin, Differential regional decline in dopamine receptor availability across adulthood: linear and nonlinear effects of age, Hum. Brain Mapp. 40 (2019) 3125–3138, https://doi.org/10.1002/hbm.24585.
[41] A. Ledonne, N.B. Mercuri, Current concepts on the physiopathological relevance of dopaminergic receptors, Front. Cell. Neurosci. 11 (2017) 27, https://doi.org/10.3389/fncel.2017.00027.
[42] J.H. Kordower, C.W. Olanow, H.B. Dodiya, Y. Chu, T.G. Beach, C.H. Adler, G. M. Halliday, R.T. Bartus, Disease duration and the integrity of the nigrostriatal system in Parkinson's disease, Brain 136 (2013) 2419–2431, https://doi.org/10.1093/brain/awt192.
[43] J.F. Leckman, M.H. Bloch, M.E. Smith, D. Larabi, M. Hampson, Neurobiological substrates of Tourette's disorder, J. Child Adolesc. Psychopharmacol. 20 (2010) 237–247, https://doi.org/10.1089/cap.2009.0118.
[44] L.F. Ferrari, J. Pei, M. Zickella, C. Rey, J. Zickella, A. Ramirez, N.E. Taylor, D2 receptors in the periaqueductal gray/dorsal raphe modulate peripheral inflammatory hyperalgesia via the rostral ventral medulla, Neuroscience 463 (2021) 159–173, https://doi.org/10.1016/j.neuroscience.2021.03.035.
[45] B. Kim, S. Yoon, R. Nakajima, H.J. Lee, H.J. Lim, Y.K. Lee, J.S. Choi, B.J. Yoon, G. J. Augustine, J.H. Baik, Dopamine D2 receptor-mediated circuit from the central amygdala to the bed nucleus of the stria terminalis regulates impulsive behavior, Proc. Natl. Acad. Sci. U. S. A. 115 (2018) E10730–E10739, https://doi.org/10.1073/pnas.1811664115.
[46] J.W. Mink, The basal ganglia and involuntary movements: impaired inhibition of competing motor patterns, Arch. Neurol. 60 (2003) 1365–1368, https://doi.org/10.1001/archneur.60.10.1365.
[47] M. Rossi, G. Giorgi, Domperidone and long QT syndrome, Curr. Drug Saf. 5 (2010) 257–262, https://doi.org/10.2174/157488610791698334.